Journal Pre-proof

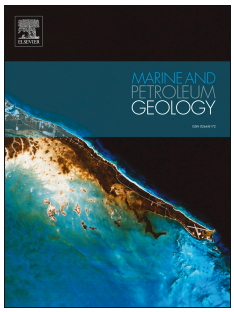

Microbial cycling, migration and leakage of light alkanes in the Nile Delta tertiary fan

U. Böker, T.A. Dodd, T. Goldberg, A.C. Aplin

PII: S0264-8172(20)30361-5

DOI: https://doi.org/10.1016/j.marpetgeo.2020.104578

Reference: JMPG 104578

To appear in: *Marine and Petroleum Geology*

Received Date: 2 April 2020

Revised Date: 2 May 2020

Accepted Date: 2 July 2020

Please cite this article as: Böker, U., Dodd, T.A., Goldberg, T., Aplin, A.C., Microbial cycling, migration and leakage of light alkanes in the Nile Delta tertiary fan, *Marine and Petroleum Geology* (2020), doi: https://doi.org/10.1016/j.marpetgeo.2020.104578.

Ulf Böker: Conceptualization, Investigation, Methodology, Formal Analysis, Software, Data Curation, Visualization, Writing – Original Draft, Writing – Review & Editing

Tim Dodd: Conceptualization, Resources, Methodology, Validation

Andrew Aplin: Project Administration, Funding Acquisition, Conceptualization, Resources, Supervision, Validation, Writing – Review & Editing

Tatiana Goldberg: Investigation, Validation, Writing – Review & Editing

Microbial cycling, migration and leakage of light alkanes in the Nile Delta Tertiary Fan

U. Böker[1,*], T.A. Dodd[2], T. Goldberg[3], A.C. Aplin[4]

[1]School of Natural and Environmental Sciences, Newcastle University, Newcastle upon Tyne, NE1 7RU, United Kingdom
[2]Broadlands Cottage, Petworth Rd, Chiddingfold, Godalming, GU8 4SU, United Kingdom
[3]Earth Surface Geochemistry, German Research Centre for Geosciences, Telegrafenberg, 14473 Potsdam, Germany
[4]Department of Earth Sciences, Durham University, Durham, DH1 3LE, United Kingdom
* Corresponding author. Present address: Department for Subsurface Evaluation, PanTerra Geoconsultants B.V., Weversbaan 1, 2352 BZ Leiderdorp, The Netherlands. Tel.: +31 715 813 505. E-mail address: u.boeker@panterra.nl.

Abstract

We present a geochemical dataset which helps unravel the complex set of processes by which light alkanes are sourced, charged, mixed, leaked and altered in the Plio-Pleistocene Nile Delta. Thermogenic gas derives from a sub-Messinian source and mixes with microbial, hydrogenotrophic, methane-rich gas in the Plio-Pleistocene section. There is strong isotopic evidence for both microbial generation and microbial degradation of ethane and propane, but these signals are only recorded where the rates of biological processes outstrip the rate of thermogenic charge. High resolution gas geochemistry profiles through four, 500-1100 m sequences of mixed channel, channel levee, mass flow deposits and hemipelagites shed light on migration and leakage pathways. We see limited geochemical evidence for migration along or across faults which cross-cut mud-rich sequences. Lateral migration along sands/silts delivers gas to structural highs, where leakage occurs vertically along focussed pathways through heterogeneous mud-rich sediments. We propose that *in situ* generation of microbial gas within mud-rich sequences facilitates percolation of migrating gases that replenishes C2+ components and sustains the biodegradation pathway in syntrophic microbial communities. High resolution changes in gas composition suggest an unequilibrated system which is being actively charged. In some structures, rates of charge and of microbial alteration of gas are broadly similar; in others, rates of charge exceed rates of microbial alteration. Our results have important implications for the understanding of both basin-wide fluid flow and the ecology of the deep biosphere.

Keywords: microbial gas, thermogenic gas, methanogenic biodegradation, genetic gas mixing, alkane carbon isotopes, hydrocarbon migration, Nile Delta

1 Introduction

The Nile Delta petroleum province is characterized by thermogenic hydrocarbons that migrate upwards across the 80°C isotherm and enter the deep biosphere (Vandré et al., 2007). In the Western province, this marker temperature lies at about 3 km burial depth and coincides with the top of salt and sabkha deposits of the Messinian Salinity Crisis (Figure 1). The Messinian is a regional barrier to cross-stratigraphic fluid exchange (Dolson et al., 2001; Loncke et al., 2004), generally restricting migration into the microbial habitat of the Plio-Pleistocene delta slope-turbidite deposits. However, gravity tectonics, halokinesis, basement fault reactivation, intra-Messinian fluid escape structures, emplacement of mud volcanoes and, regionally, the position of the Messinian eroded shelf edge, generate a range of pathways by which gas bypasses the salt deposits (Loncke et al., 2006; Garfunkel, 1998; Abd-Elfattah & Fahmy, 2017; Eruteya et al., 2015; Bertoni et al., 2013). These pathways can be placed into the broader structural and stratigraphic configuration of the offshore Nile Delta basin by reference to Hanafy et al. (2017).

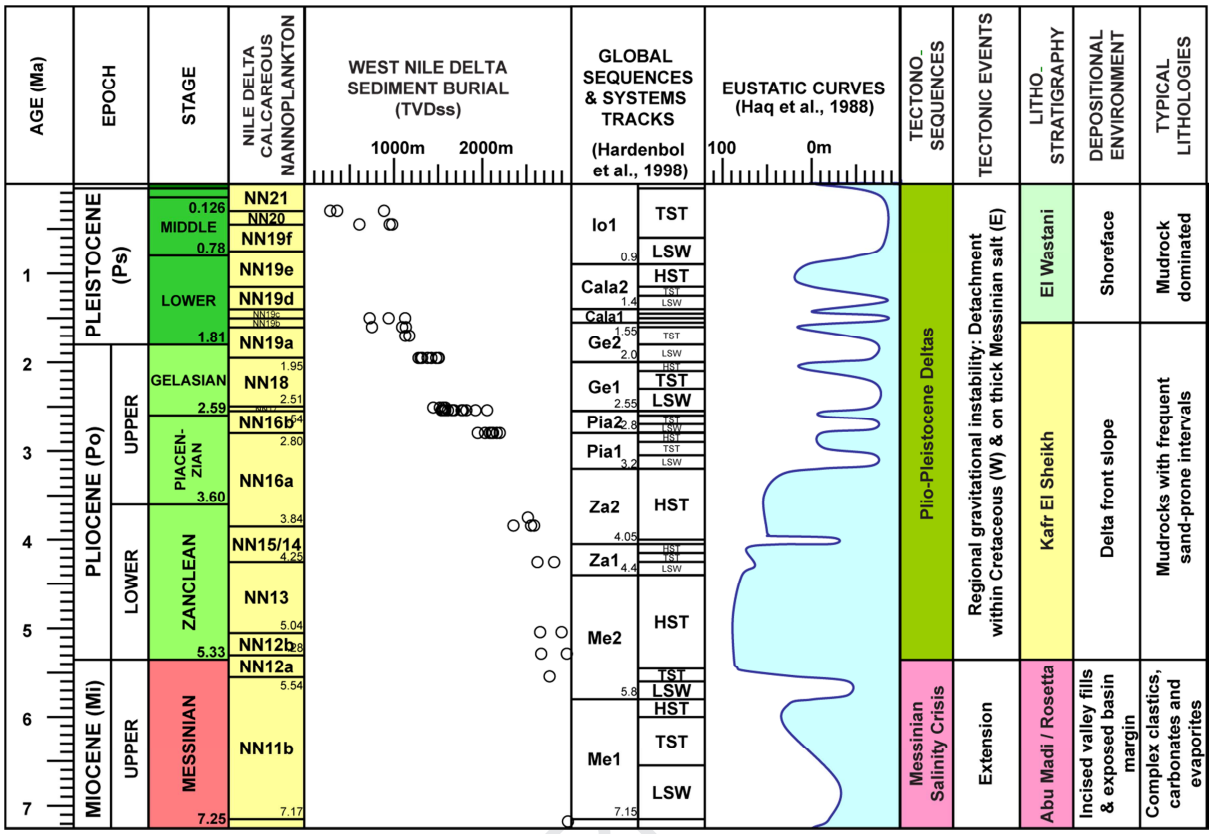

Figure 1 Nile Delta stratigraphic panel with tectonic and lithological framework. Most of our gas dataset was sampled at 1-2 km burial depth in the Pliocene Kafr El Sheikh Formation.

1.1 Source rocks and migration routes

The Pliocene section is immature throughout the offshore Nile Delta (El-Ella, 1990; Abdel Aal et al., 2000; Vandré et al., 2007). Oligocene-Miocene source rocks in the Nile Delta and Eastern Mediterranean are of type-III and mixed type-II/III kerogen (Kamel et al., 1998; Sharaf, 2003; El Nady, 2007; Vandré et al., 2007; Keshta et al., 2012; Khaled et al., 2014) and are commonly considered to be the main contributor to the regional Pliocene gas and condensate fields (Abdel Aal et al., 2000). While peak generation in the onshore Nile Delta area occurred in the Late Miocene (Kamel et al., 1998), source rocks in the offshore part only entered the early-mature stage in the Pleistocene (Shaaban et al., 2006; Vandré et al., 2007). Biomarker studies by El Diasty & Moldowan (2013) suggest that although the generally Late Cretaceous to Tertiary source rocks contain varying proportions of bacterial, terrestrial and algal organic matter, they can be broadly characterized by terrestrial type-III kerogens with present maturities around 0.7-0.8 %Ro. Basin modelling in our study area confirms that the Oligocene at 5-6 km burial depth falls in that maturity window (Vandré et al., 2007). This depth and maturity range appears to confirm that the main source of thermogenic charge in the offshore Nile Delta area can be narrowed down to Chattian turbidites and deeper marine systems of the Rupelian (Villinski, 2013). However, contributions from regional Mesozoic sources – ranging from Late Cretaceous-Eocene (type-II) to Late Jurassic-Middle Cretaceous in age (type-II/III; Sharaf, 2003; Feinstein et al., 2002; Al-Balushi et al., 2016) – cannot be completely ruled out (Villinski, 2013). These are compatible with the source of gases sampled by Mastalerz et al. (2007) at the Isis mud volcano in the central offshore Nile Delta. The relatively low maturity-depth gradient in the Nile Delta basin is caused by rapid sediment burial (ca. 460 m/Ma) at moderately high heating rates (15±2 °C/Ma) (Böker, 2011; Quigley et al., 1987).

Fluid migration from the sub-Messinian sources results in the mixed microbial-thermogenic Pliocene gas and condensate accumulations that are of commercial interest today (Vandré et al., 2007). It has been suggested that migration is focussed along pre-Messinian normal faults and Pliocene growth

faults, with up-dip lateral migration and re-migration facilitated by the presence of slope channels, Messinian valleys and unconformities (Kamel et al., 1998; Loncke et al., 2004; Khaled et al., 2014). In some areas, bypass structures such as mud volcanoes and gas chimneys also act as focussed conduits for gas migration to the seabed (Loncke et al., 2004; Loncke et al., 2006; Mastalerz et al., 2007; Mastalerz et al., 2009; Dupré et al., 2010).

1.2 Gas geochemistry

In this paper, we use the chemical and isotopic composition of natural gas to place constraints on its origin, migration and leakage. In the Pliocene of the Nile Delta, gas is often a mixture of thermogenic and microbial sources, so it is important to characterise the composition of primary gases and the ways in which those compositions are altered by secondary processes. These processes, and the range of chemical and isotopic compositions associated with them, are outlined in Table 1. The composition of thermogenic gas mainly reflects the nature and maturity of the source rock (Clayton, 1991; Berner & Faber, 1996). In the Nile Delta, the geochemical fingerprint of thermogenic gas can be seen in Pliocene slope channel reservoirs where commercial accumulations of gas are compositionally wetter (C1 ≈ 90%) and isotopically heavier (δ^{13}C1 ≈ -40 ± 1‰) than microbial gas (Vandré et al., 2007). Microbial gases have the chemical signature of methanogenesis (C1 > 99%; δ^{13}C1 ≤ -60‰; Whiticar, 1999; Vinson et al., 2017).

The formation of primary thermogenic and microbial gases is subject to a kinetic isotope effect (KIE) in which lighter isotopes (e.g.^{12}C) react faster than their heavier counterparts (e.g. ^{13}C) as a result of differences in mobility and bond strength (Chung et al., 1988; Coleman et al., 1981). Both thermal cracking and biosynthesis result in a lighter carbon isotope signature of the product relative to the organic precursor. The isotope separation between thermogenic gas and its kerogen precursor is largest at the early stage of gas generation and decreases over time as the isotopic composition of the source decreases (Chung & Sackett, 1980). The direct precursor of methanogenic gas is most commonly CO_2 but can also be organic acids; the latter also involves ethanogenesis and propanogenesis (Table 1). The relative importance of precursor CO_2 and organic acids depends on the carbon supply from sedimentary organic matter (Yoshioka et al., 2015) and petroleum biodegradation (Jones et al., 2008). A more comprehensive review of methanogenic pathways in conjunction with biodegradation is summarised in Vinson et al. (2017). Vandré et al. (2007) suggested that the most common secondary geochemical overprint of gases sampled in the Nile Delta is related to the biodegradation of thermogenic wet gas components, i.e. anaerobic microbial oxidation of hydrocarbons to CO_2 (Jones et al., 2008; Milkov, 2011). This process is commonly observed in C3+ normal hydrocarbons (James & Burns, 1984; Kinnaman et al., 2007) where it leaves a heavy δ^{13}C footprint in the residual hydrocarbon species (Table 1), due to a microbially driven kinetic isotope effect.

		HC generation						HC alteration			
		catagenesis	microbial mediation			coupled		segregative migration [v]			
		thermogenic alkanes	acetoclastic methanogenesis [e] & alkanogenesis [b]		hydrogenotrophic methanogenesis	methanogenic biodegraded alkanes	biodegraded alkanes	diffused alkanes	adsorption-stripped free alkane phase	desorbtion-charged free alkane phase*
depositional setting (observed)		high TOC rocks	freshwater [c]	marine [b], freshwater [a]	marine [c]	marine [e]	marine, freshw. [w]	n.a.	n.a.	n.a.
environmental conditions		thermal maturity	anaerobic, sulphate-free [c,x]	anaerobic, variable sulphate levels [a,b]	anaerobic, sulphate-free [c,x]	anaerobic, variable sulphate levels [e]	anaerobic, sulphate-poor [w,x]	chemical gradient	clay and/or organic matter	PVT changes
process		thermal cracking (catagenesis)	acetate fermentation [c,d,p]		carbonate reduction [c,e]	microbial oxidation & methanogenesis	microbial oxidation	diffusion	adsorption	desorbtion
net reactants		K, OM, HC	CH_3COOH	$CH_3COOH+3H_2$	$196H_2+64CO_2$	$4C_{16}H_{34}+30H_2O$	$4C_{16}H_{34}+128H_2O$	n.a.		
net products		(lighter) HC	CH_4+CO_2	$C_2H_6+2H_2O$	$C_3H_8+4H_2O$	$49CH_4+15CO_2$	$64CO_2+196H_2$			
substrate / organic precursor		mature organic matter	recent (recalcitant) organic matter [y]		$49CH_4+15CO_2+98H_2O$	petroleum or bitumen	petroleum, bitumen or labile kerogen			
oxidant		no redox	acetate		recent organic matter	HC species	HC species			
reductant			hydrogen	hydrogen	CO_2	water	water			
(by)produced C species		C1+	C1 – C3 [b,e]		hydrogen	C1 and CO_2 [g]	CO_2			
C1 (vol.%)		≤ 98 [j]	>99 [a]		C1	enriched (active)	enriched (passive)	enriched [n]	enriched [o]	depleted [o]
C2 (vol.%)		Σ$C2+ ≥ 2$ [j]	3e-4 – 0.9 [a]		>99 [a]	n.p.	consumed [h]	→ 50% less eff. than C1 [p]	preferentially depleted [o]	preferentially enriched [o]
C3 (vol.%)			<1e-3 [s]		n.p.			negligible with decreasing solubility		
nC4 (vol.%)			n.p.				relative stable [i]			
iC4 (vol.%)							consumed [h]			
C5+ (vol.%)										
CO_2 (vol.%)		produced	produced	n.r.	consumed	consumed (net) [e,q]	produced	enriched [ab]	n.d.	n.d.
$\delta^{13}C1$ (‰)		-43 – -28 [k], -50 – -20 [c]	-70 – -50 [c,q]		-110 – -55 [c,q]	-70 – -40 [u], ≤ -55 [r, g]	increase [c]	decrease [n]	decrease [o]	increase [o]
$\delta^{13}C2$ (‰)		-36 – -23 [k]	-73 – -45 [s]		n.p.	n.p.	increase [h]	negligible with increasing carbon chain length		
$\delta^{13}C3$ (‰)		-32 – -21 [k]	n.d. [t]							
$\delta^{13}nC4$ (‰)		-31 – -20 [l]	n.p.				relative stable [i]			
$\delta^{13}iC4$ (‰)		-31 – -20 [l,m]					increase [h]			
$\delta^{13}C5+$ (‰)		-30 – -19 [l]								
$\delta^{13}C\text{-}CO_2$ (‰)		-25 – -20 [f]	-30 – 0 [c]		increase; -30 – +20 [c]	increase (net); -21 – +20 [e,q,u]	decrease; <-40 – -25 [e,f]	decrease [z]	increase [aa]	decrease [aa]
$\Delta^{13}C$ (substrate - C1) (‰)		0 – 30 [c]	25 – 35 [c]		49 – 95 [c]	16 – 33 [u]	n.r.	n.r.	n.r.	n.r.
$\Delta^{13}C$ ($C1_{initial}$ - $C1_{final}$) (‰)		7 – 30 [k,c]	n.r.		n.r.	net positive	5 – 25, general <10 [c]	max. -20 [n]	max. -20 [o]	max. +20 [o]

*Table 1 Overview of processes that contribute to the signature of hydrocarbon species in sulphate-free environments of the deep subsurface. Legend: n.a. not applicable, n.d. not determined, n.p. not produced, n.r. no reaction, *e.g. headspace gases such as from degassing drill cuttings, HC hydrocarbons, K kerogen, OM organic matter, PVT pressure-volume-temperature. [a] (Davis & Squires, 1954; Oremland et al., 1988); [b] (Hinrichs et al., 2006); [c] (Whiticar, 1999); [d] (de Graaf et al., 1996; Wellsbury et al., 1997; Vieth et al., 2008); [e] (Jones et al., 2008); [f] (Milkov, 2011); [g] (Zengler et al., 1999; Pallasser, 2000); [h] e.g. (Stahl, 1977; Chung et al., 1988); [i] (Kniemeyer et al., 2007) (for sulphate-rich conditions); [j] (Fuex, 1977; Rice & Claypool, 1981; James, 1983; Mattavelli et al., 1983; Schoell, 1983; England, 1990; Schoell et al., 1993); [k]*

(Berner & Faber, 1996), data envelope for type-II & type-III kerogen with δ13C(kerogen) = -26.5‰ in VR range from 0.6 to 2.0 %Ro; [l] (Chung et al., 1988); [m] (Böker, 2011); [n] e.g. (Galimov, 1975; Fuex, 1980; Pernaton et al., 1996; Prinzhofer & Pernaton, 1997; Zhang & Krooss, 2001); [o] (Friedrich & Jüntgen, 1972); [p] (Krooss, 1986; Nelson & Simmons, 1992); [q] (Katz, 2011); [r] (Lückge et al., 2002); [s] (Taylor et al., 2000) ; [t] (Schloemer et al., 2016); [u] (Feisthauer et al., 2010); [v] (Prinzhofer et al., 2000); [w] (Aitken et al., 2004); [x] (Head et al., 2003); [y] (Wellsbury et al., 1997); [z] (Cerling et al., 1991; Risk & Kellman, 2008); [aa] (Larson & Breecker, 2014); [ab] (Weissman & DuBro, 1971; Lide, 2005).

1.3 Rationale and aim of this study

Within the general geochemical and fluid flow framework outlined above, this paper presents a geochemical dataset of unprecedented size and resolution with the aim of unravelling the complex set of processes by which light alkanes are sourced, charged, leaked and altered in a delta slope setting. The results generate insights not only to the microbial processes occurring in the deep biosphere, but also the pathways by which hydrocarbon gases migrate and leak through a mud-rich slope sedimentary system comprising hemipelagites, mass flow deposits, channels and channel levees. The data also allow consideration of the relative rates of gas flux and microbial alteration.

The paper is divided into three main sections. Firstly, we perform a strict quality control assessment of the gas compositions, since these can be seriously compromised by sampling artefacts. Secondly, we bring together a very large set of gas data in order to identify the chemical and carbon isotopic composition of the main sources of the region's primary thermogenic and microbial gas. This is based on an understanding of the many factors which influence the composition of both thermogenic and microbial gas (Table 1). By identifying the composition of the microbial and thermogenic gas, we then quantify the mixing of compositional end-member gases and identify the secondary microbial processes which alter the chemical and isotopic composition of thermogenic gas.

In the third part of the paper, we interpret geochemical profiles of gas samples taken at least every 10 m through 400-1100 m sections of four wells which penetrate series of mud-rich and sand-rich slope sediments. These data generate insights into vertical, lateral and fault-related migration and leakage pathways, and give some information about the relative rates of both charge and the microbial processes which occur in the deepest biosphere.

2 Sampling and quality control

BP provided a comprehensive wellsite dataset from 25 boreholes, drilled over an offshore area of 4000 km² and with Pliocene sections of typically 2-3 km length. Sample locations are displayed in Figure 2.

Most data used here represent gases sampled from the mud system of the wells whilst drilling. The boreholes were drilled with a mineral oil-based mud circulation system and gases were extracted from the mud using an agitator-type gas trap positioned in the possum belly of the mud shakers. An unheated gas trap was used. The wellsite system used a flame ionisation detector (FID) column gas chromatograph to distinguish C1 to C5 gases, fully resolving C1 to C5 branched and normal alkanes and partially resolving alkenes. FID measurements are run for operational safety and typically no isotope data are collected. However, these continuous gas logs can be used for careful depth matching of all mudlog data, including flowline gas samples against wireline logs (Böker, 2011).

Isotube samples were taken at regularly spaced depth intervals over the wells, as close as 3m in expected reservoir sections and up to 10m in intervals lacking potential reservoir. These samples are taken from the gas line into the logging unit. The high sampling density generates several sets of isotube data within a single reservoir unit, allowing trends to be seen in the data as well as showing

outliers due to occasional leakage from isotube sample containers. The lighter ^{12}C isotope leaks preferentially and results in isotopically heavy outliers in the residual gas sample.

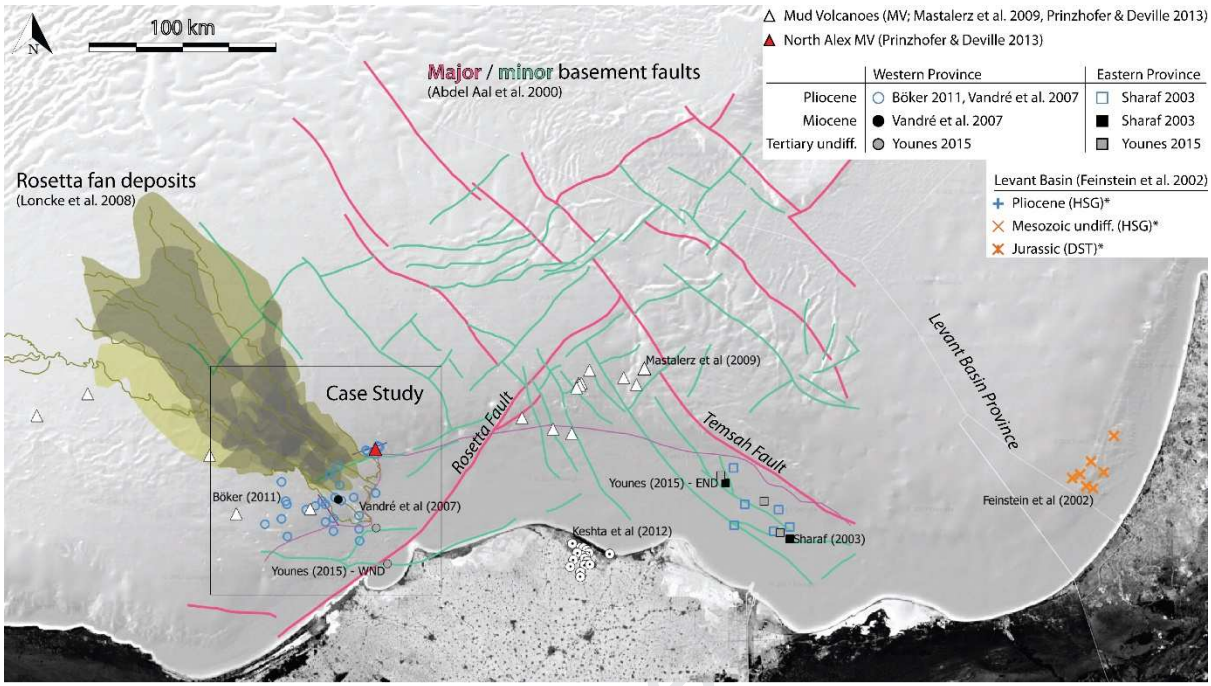

*Figure 2 Overview map of the Nile Delta Tertiary fan with location of the case study area in the Western Province (Figure 10) and data from offset locations in the Eastern Mediterranean (Eastern Province and Levant Basin). For the purposes of this study, we define the boundary between Western and Eastern Province longitudinal to the meeting point of the Rosetta and Temsah faults. All location markers refer to gas samples except for the onshore maturity study of Keshta et al. (2012). *Note that, in this figure only, sample locations in the Levant Basin are plotted indiscriminate of stratigraphic unit due to cross-stratigraphic well sampling. Satellite imagery courtesy of Google.*

In addition, canned headspace gas (HSG) samples were taken at a lower sampling density. These samples consist of drill cuttings taken at regular intervals and placed in sealable cans. The cans are filled to about one third with cutting material and covered with water with added bactericide. The gas diffuses into the headspace volume of the cans and is then analysed both compositionally and isotopically. The HSG sampling method is known for desorption-related isotope fractionation effects and diffusive loss of methane during storage (Risk & Kellman, 2008). The advantage of isotubes over headspace samples is that isotubes extract fluids from the produced drill mud in a closed-system environment prior to atmospheric exposure at the mud shaker.

Gases released into the mud system are thought to be mainly from the pore volume of the rock as it is broken up by the drill bit and depressurized as cuttings are brought to atmospheric PT conditions. Gases that accumulate in the headspace of sealed cans certainly contain a proportion of similar gases released from the pore volume but may also contain gases adsorbed onto mineral and organic surfaces in the rock.

When the composition of gases sampled during drilling is compared to those taken from wireline formation sampling (e.g. Modular Formation Dynamics Tester, MDT) and by pump testing (e.g. Drill Stem Tests, DST), a variety of issues need to be considered. The principal issue in oil-based mud systems is solution of gases into the drilling mud, potentially leading to the occurrence of recycled gases in re-injected muds. Recycling is most likely to be seen when drilling past a highly gas-saturated reservoir section into underlying mudstones with low gas contents, resulting in fingerprints from the reservoir section persisting into the mudstones.

The effects of solution of hydrocarbons into the mud system are most pronounced for higher molecular weight hydrocarbons, especially at low temperatures. This causes isotube samples to have lower C2+ concentrations than *in situ* gases that are best represented by MDT sampling. Figure 3a-d

shows a comparison of C1-C4 compositions in isotube and HSG gases compared to MDT samples taken within 10m of the flowline samples and gives some idea of the scale of the compositional difference. Isotube samples tend to contain less C2+ than other sampling techniques, which we assume represents the preferential loss of C2+ through dissolution into the mud system. HSG samples have the highest C2+ concentrations, which we interpret as being due to preferential loss of methane during sampling. The magnitude of isotope fractionation in HSG samples can be seen in Figure 3e-f for methane and ethane, respectively. In contrast, the same figures show that wet gas recycling as captured by isotube sampling does not lead to systematic isotope fractionation between *in situ* gases and the mud system. We conclude that both isotube and MDT samples can be used as a proxy for *in situ* gases.

Carbon isotope data for methane in samples with less than 1000 ppm methane were removed from the dataset and not interpreted. Similarly, no data were interpreted where the abundances of C2, C3 and C4 were less than 5 ppm. The final compositional dataset comprises 62 MDT samples and 748 isotube samples from 20 boreholes that penetrate 12 separate hydrocarbon accumulations. The original isotope database contained 434 analyses, all of which had at least the methane carbon isotope ratio ($\delta^{13}C1$) determined by Isotech Laboratories Inc.. The quality control described above left 77% (n=333) of all methane isotope analyses, 72% (n = 234) of all ethane, 59% (n = 84) of propane, 63% (n = 81) of iso-/normal butane and 100% (n = 3) of iso-/normal pentane for this study.

As the wells were all drilled using the same rig with the same gas acquisition system, the subset of gas samples that passed the stringent quality control for this study is a robust and internally consistent set of data. Some previously published data from the region are also shown in Figure 2. Note that the headspace gas analytical results from Feinstein et al. (2002) have error bars that reflect the quality concerns discussed above; DST data from Jurassic gases are used for plotting unaltered thermogenic gas properties. All raw data are available in the public domain (Böker, 2011).

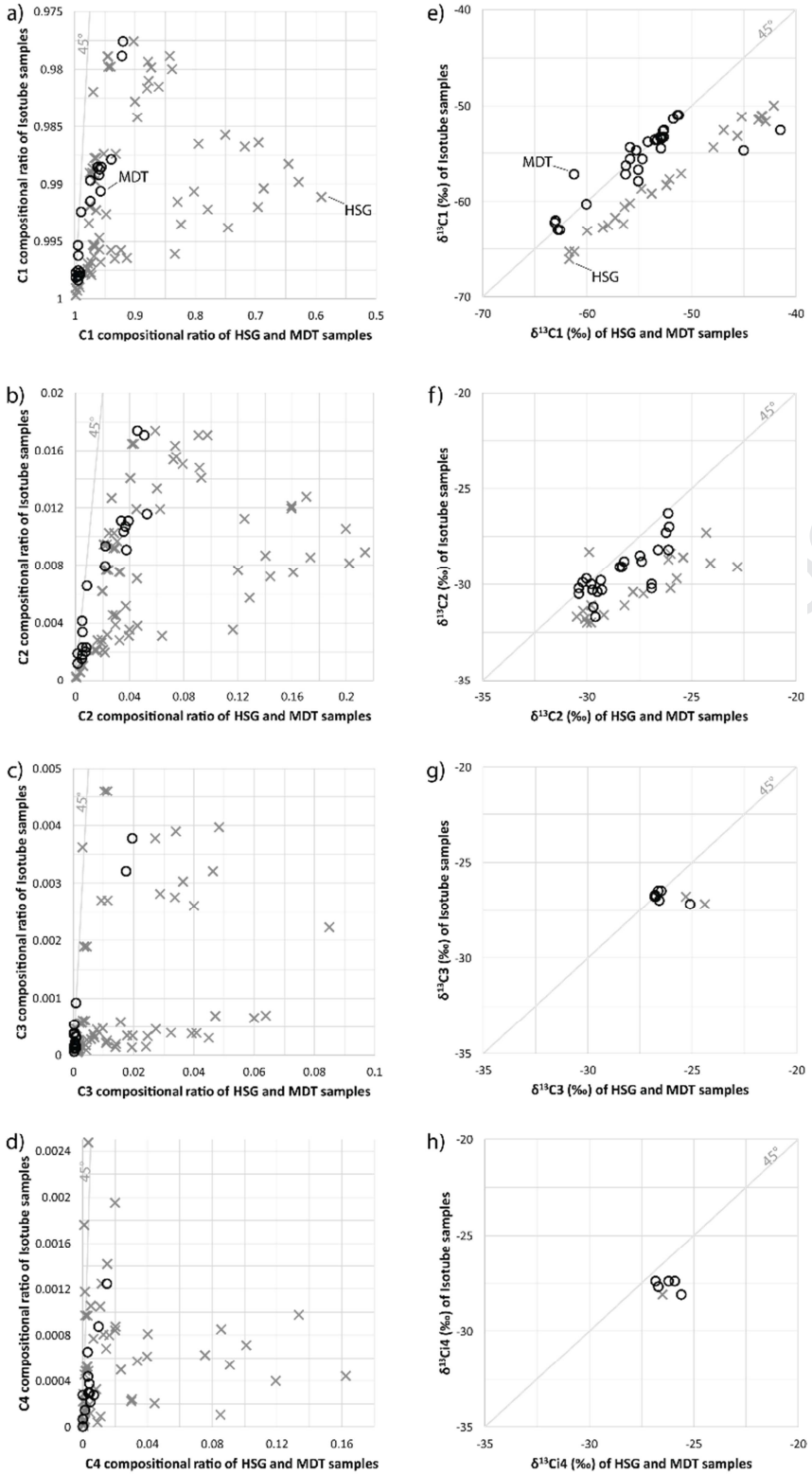

Figure 3 Cross-plots comparing compositional ratios (a-d; methane to butane system) and carbon isotope ratios (e-h) from analytical results of different gas sampling techniques. Samples were compared if taken within 10m depth after depth-matching flowline samples (isotube and HSG) with MDT reference depth (logger's depth, see Böker, 2011). Using isotube analyses as the benchmark (y-axes), both HSG (grey crosses) and MDT (empty circles) data tend to plot on the right hand side of the 45° line, indicating preferential loss of methane in HSG samples and C2+ losses to the mud system in isotube samples (a-d). Most notably, HSG show heavier carbon isotope ratios in methane (e) and ethane (f), whereas isotube gases show no or little fractionation relative to the MDT benchmark; this may be partly due to the higher resolution of MDT compared to flowline sampling. Compositional outliers and the systematic isotope offset indicate an intrinsic sampling problem with HSG data. We thus limit our study to the joint interpretation of MDT and isotube gas samples. See text for further discussion.

3 Geochemical signatures of alkanes in the Nile Delta subsurface

In this section we discuss the processes that lead to the range of geochemical signatures observed in our bulk gas data set. We (i) present the data within previously published genetic fields for gas composition (Section 3.1); (ii) identify primary gas signatures of methanogenic and thermogenic end-members (Section 3.2); (iii) determine the geochemical footprints of biodegradation in the methane-ethane system (Section 3.3); and (iv) consider trends in the carbon isotope ratios of CO_2 and C2+ in the context of methanogenic biodegradation (Section 3.4). These observations of biogeochemical processes then provide the interpretational framework for an assessment of both microbial cycling and migration of gases in two case studies in Section 4.

3.1 Genetic fields

Since the late 1970s cross-plots of molecular ratios and stable isotopic compositions have been utilized to empirically classify the origin, maturity and alteration history of natural gases. In Figure 4, we plot our data in the genetic field envelopes published by Milkov & Etiope (2018), who we refer to for a detailed account of the history and evolution of gas diagrams.

In the Bernard-type display (Figure 4a,d), gases plot on the U-shaped trend from primary microbial to early and late mature thermogenic. The bulk of the data lie in the transition zone between gases of microbial and thermogenic origin. Hydrogen isotopes of methane (δD1 in Figure 4b,e) suggest that CO_2 reduction ("carbonate" reduction in Table 1) is the dominant metabolic pathway for primary microbial gas, with the caveat that hydrogen isotopes are known to be susceptible to exchange with formation water (Schimmelmann et al., 1999; Vinson et al., 2017). The bulk of the data falls on a straight mixing line that connects the field of CO_2 reduction (low $\delta^{13}C1$) with the thermal maturity line (high $\delta^{13}C1$) in Figure 4e. We infer that the microbial and thermogenic end-members have distinct primary source signatures so that variations in the gas composition are dominated by mixing rather than by variations in source compositions. Data points that deviate from the dominant mixing trend in Figure 4b,e exhibit very low δD1 indicative of acetate fermentation (Table 1), which is a metabolic pathway that is coupled with CO_2 reduction during methanogenic biodegradation (Jones et al., 2008). Here, methanogenic biodegradation is the main source of secondary microbial gas (Table 1).

$\delta^{13}C\text{-}CO_2$ is a particularly sensitive indicator of biodegradation processes, as shown by a significant proportion of gases that deviate from the ideal mixing line between primary microbial and thermogenic fields (Figure 4f). In Figure 4f, the position and curvature of the biodegradation pathways depends on the initial composition of each gas mixture before it was biodegraded (Jones et al., 2008). We have plotted the data envelope of various open (Boreham et al., 1998), semi-open (Takahashi & Suzuki, 2017) and closed system (Andresen et al., 1995; Takahashi et al., 2014; He et al., 2018) pyrolysis results from Mesozoic and Tertiary type-III source kerogen in Figure 4f. The solid red line denotes the maturity trend of the semi-open system in the vitrinite reflectance range from 0.6 to 1.6 %Ro (Takahashi & Suzuki, 2017). The scatter of the remaining pyrolysis results is within the hashed white field because the measured isotope trends are more varied than the results from Takahashi & Suzuki (2017). All pyrolysis data are corrected for the initial carbon isotope ratio of the source kerogen. The pyrolysis data demonstrate that CO_2 carbon isotope effects related to the thermal maturation of type-III source kerogen are less than those suggested by the universal genetic fields from Milkov & Etiope (2018). A smaller range of thermogenic $\delta^{13}C\text{-}CO_2$ can be expected where gas is generated from a relatively uniform source kerogen. This is the case in the Nile Delta, given the long-lived nature of the depositional setting and sediment source over a period of 5Ma (Figure 1), with terrestrial input from higher plant material as opposed to e.g. Carboniferous coals (Takahashi et al., 2014; Takahashi & Suzuki, 2017).

Note that the extremely low $\delta^{13}C_1$ and $\delta^{13}C\text{-}CO_2$ in some samples from mud volcanos (Figure 4a,c) suggest very shallow metabolic processes related to the oxidation of methane by sulphate-reducing bacteria (Yoshinaga et al., 2014; Knittel & Boetius, 2009).

We conclude from the genetic fields study that whilst many gases have mixed primary microbial and thermogenic sources, sulphate-free biodegradation processes are also occurring, potentially obscuring the classical gas isotope mixing signatures between primary microbial and thermogenic gases.

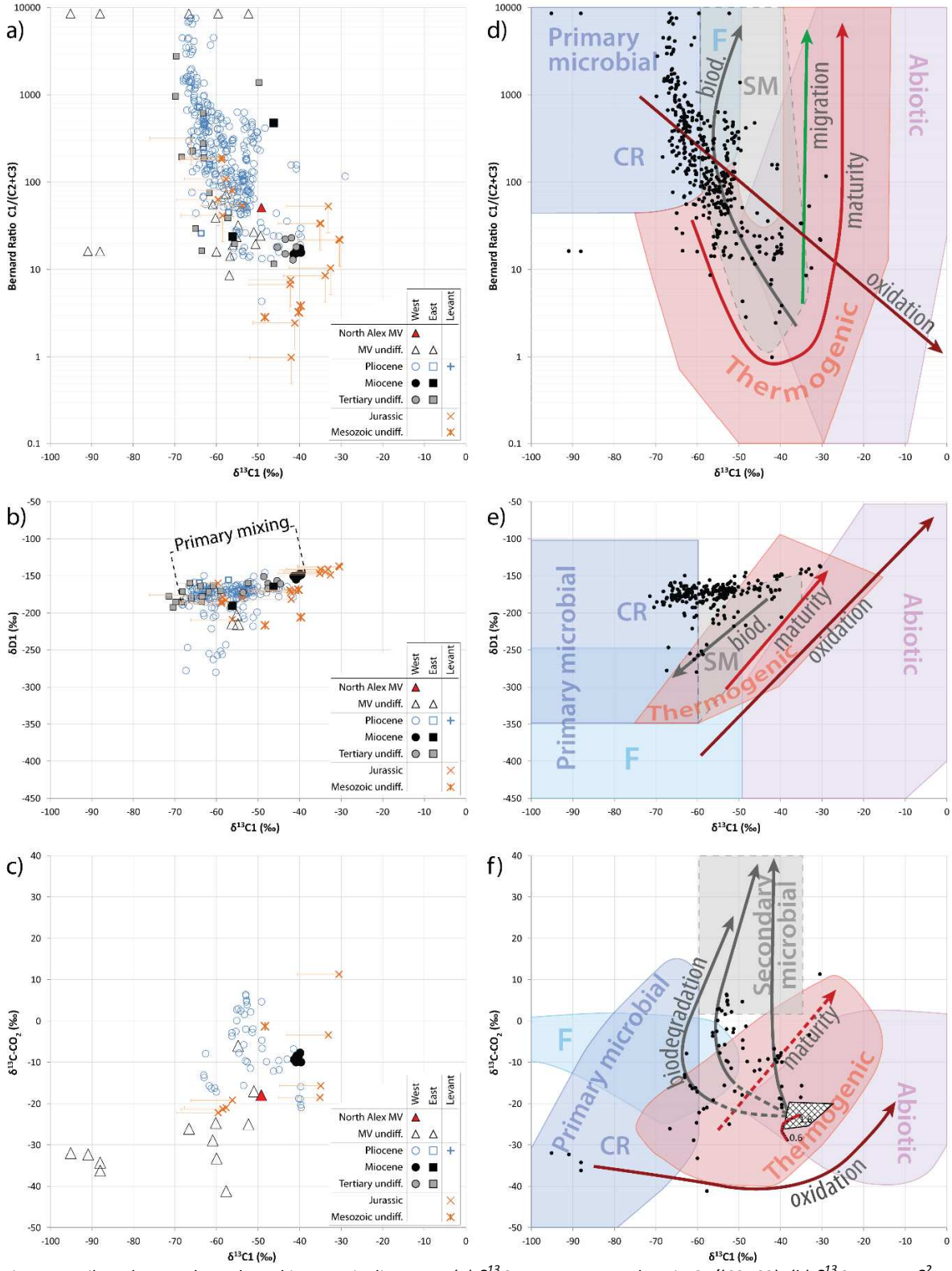

Figure 4 Nile Delta gas data plotted in genetic diagrams. (a) $\delta^{13}C1$ versus Bernard Ratio C1/(C2+C3). (b) $\delta^{13}C1$ versus $\delta^{2}H$-C1 or δD1. (c) $\delta^{13}C1$ versus $\delta^{13}C$-CO_2. (d-f) Revised genetic fields from Milkov & Etiope (2018) with biodegradation pathways (f) modified from Jones et al. (2008). CR = CO_2 reduction; F = (acetate) fermentation; SM = secondary microbial. Biod. = biodegradation. The cross-hashed field is the pyrolysis data envelope.

3.2 Primary gases

Methane is by far the most abundant hydrocarbon species in the Nile Delta Pliocene, and $\delta^{13}C1$ of thermogenic and microbial methane differs by around 30 ± 5‰ (Table 1). Microbially-derived

methane mainly occurs at temperatures lower than around 90°C (Figure 5), straddling the full temperature window of the deep biosphere (Head et al., 2003). However, entering in the realms of intense diagenesis (Chamley, 1989), there continues to be evidence for mixed microbial and thermogenic methane at temperatures up to around 140°C (Figure 5).

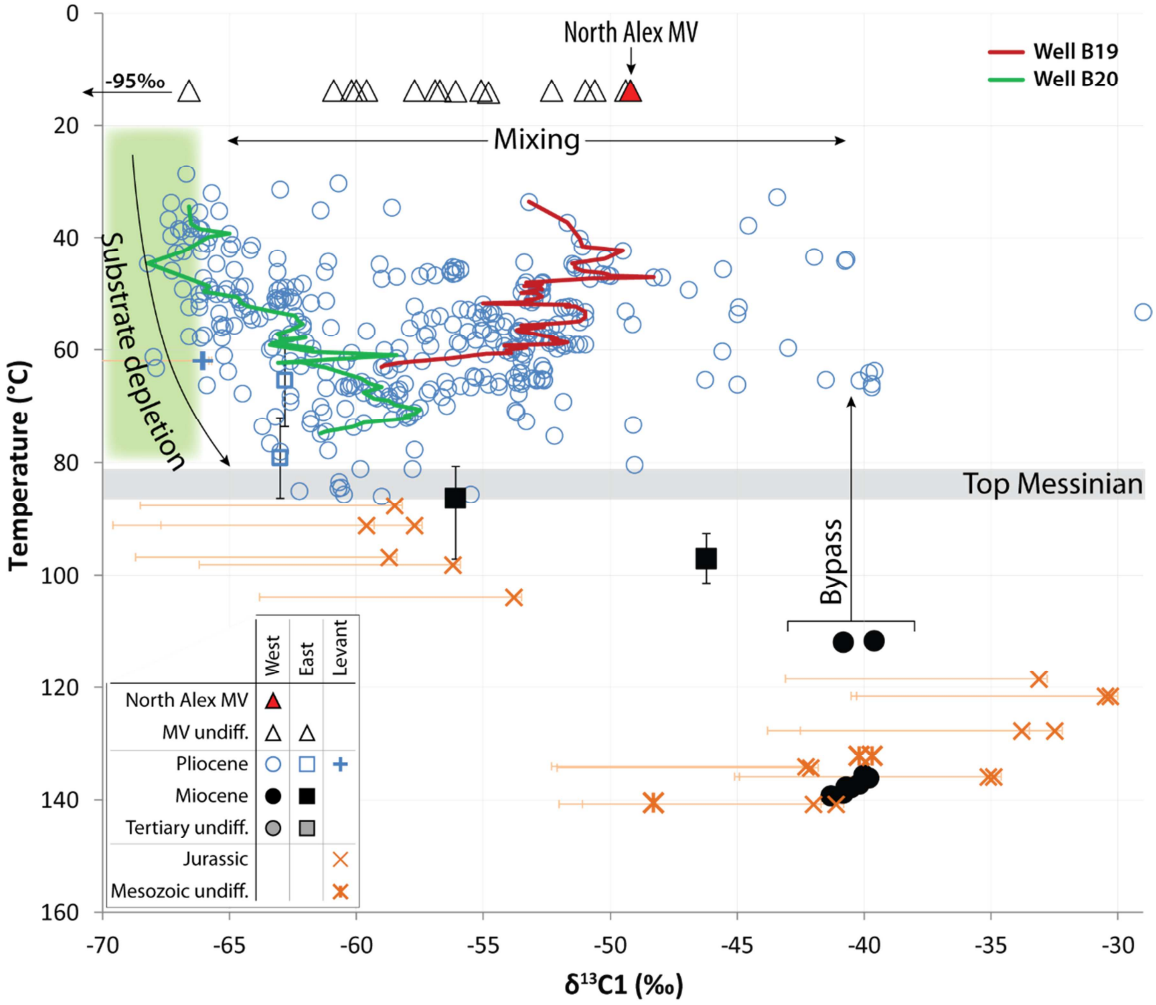

Figure 5 Distribution of methane carbon isotope signatures relative to the present-day temperature of the sampled strata in the Nile Delta and Eastern Mediterranean. Methane is isotopically lightest at low temperatures and becomes heavier at higher temperatures, related to production of methane from an increasingly isotopically heavier substrate (substrate depletion). Methane in the Miocene and older stratigraphic sections is dominated by the heavy isotope signature of thermogenic gas. Heavy $\delta^{13}C1$ within the approximate temperature range of the deep biosphere (green box) results from migration and mixing of thermogenic gases from below the regional Messinian barrier. The vertical trends in wells B19 (red line) and B20 (green line) are discussed in the Horus case study, Section 4.1. MV = mud volcano. HSG data include uncertainties (orange error bars) resulting from sampling protocols which enrich the methane in $\delta^{13}C1$ and should be treated with caution.

The presence of heavy $\delta^{13}C1$ (≈ -40‰) at low temperatures and shallow stratigraphic levels confirms that thermogenic gases bypass Messinian salts, e.g. via prominent seismic-scale structures such as reactivated basement faults and mud volcanoes (Loncke et al., 2004; Garziglia et al., 2008; Dupré et al., 2010), and/or as a result of sufficient structural focus at depth to allow for capillary failure of reservoir top seals (Aplin & Larter, 2005). The apparent $\delta^{13}C1$ signature of microbial methane increases from -68‰ at 40°C to -63‰ at 80°C, indicative of a source carbon pool that is increasingly ^{12}C depleted as a result of microbial generation of ^{12}C-rich methane. Dilution effects from early-mature (Milkov & Etiope, 2018) or "diagenetic" formation of *in situ* gases in the shallow subsurface prior to thermal degradation of kerogen (Rice & Claypool, 1981) cannot be differentiated from microbial gas generation as the reaction windows of these two processes overlap significantly (Schoell, 1983).

Mixing of microbial and mature thermogenic methane leads to intermediate $\delta^{13}C1$ values that, given the compositional dominance of methane in the primary genetic gases (Table 1), can be approximated with a linear end-member mixing model as follows:

Equation 1 $$x_t\,[f] = \frac{(\delta^{13}C1 - \delta^{13}C1_m)}{(\delta^{13}C1_t - \delta^{13}C1_m)}$$

where x_t is the fraction of thermogenic methane and $\delta^{13}C1_m$ and $\delta^{13}C1_t$ represent the pristine methanogenic and thermogenic end-member carbon isotopic ratios of methane. Since the gas system is dominated by these two primary sources, we can then estimate the fraction of each alkane species (Cn) in thermogenic-methanogenic mixtures (subscripts *t* and *m*, respectively) using Equation 2 and the end-member isotopic and chemical compositions in Table 2.

Equation 2 $$Cn_{mix}[f] = x_t * Cn_t + (1 - x_t) * Cn_m$$

Table 2 Primary gas end-members used in this study. Near-pristine microbial gas is represented by the isotopically lightest gas sample of our dataset. The thermogenic gas properties at thermal maturities of VR = 0.8 %Ro (El Diasty & Moldowan, 2013) are derived from published models (Berner & Faber, 1996; Clayton, 1991). These are calibrated with an initial carbon isotope ratio of the source kerogen at $\delta^{13}C$(kerogen-II/III) = -26.5 ‰ to ensure that the mixing lines in Figure 6 and Figure 7 intersect Miocene gas sample properties. Note that all concentrations are normalised to unity.

	$\delta^{13}C1$ (‰)	$\delta^{13}C2$ (‰)	C1 (f)	C2 (f)	C3 (f)
Microbial gas (Pliocene sample)	-68	-48	0.9995	0.0005	~0
Thermogenic calibration point (Miocene sample)	-38	-28.5	0.934	0.045	0.021
Primary thermogenic gas (type-III)	-33	-28.5	0.926	0.05	0.024
Secondary thermogenic gas (type-II)	-42	-34	0.779	0.15	0.071

Equations 1 and 2 couple relative alkane concentrations to methane carbon isotope signatures. This simple model allows a visual illustration of the mixing of purely primary gases for the Nile Delta and the Eastern Mediterranean gas samples in a Bernard-type diagram (Figure 6). Miocene gases appear to contain about 20% of methanogenic input, assuming that the primary Oligocene source rock in the study area is dominated by dispersed terrestrial organic matter with type-III kerogen (Kamel et al., 1998; Sharaf, 2003; El Nady, 2007; Vandré et al., 2007; Keshta et al., 2012; Villinski, 2013; Khaled et al., 2014). Most data plot above the ideal mixing line and mark compositional dryness that is not predicted by our primary gas mixing model. This systematic offset could be partially explained by the presence of thermogenic gas from different source rocks and/or the same source at different maturities, suggested by a few data points that are compositionally wetter than expected and that plot below the ideal mixing line in Figure 6. Another explanation of the higher than predicted C1/(C2+C3) ratios is that C2+ alkanes have been removed by secondary processes such as biodegradation. The loss of C2+ through microbial processes has been proposed previously in the Nile Delta (Vandré et al., 2007).

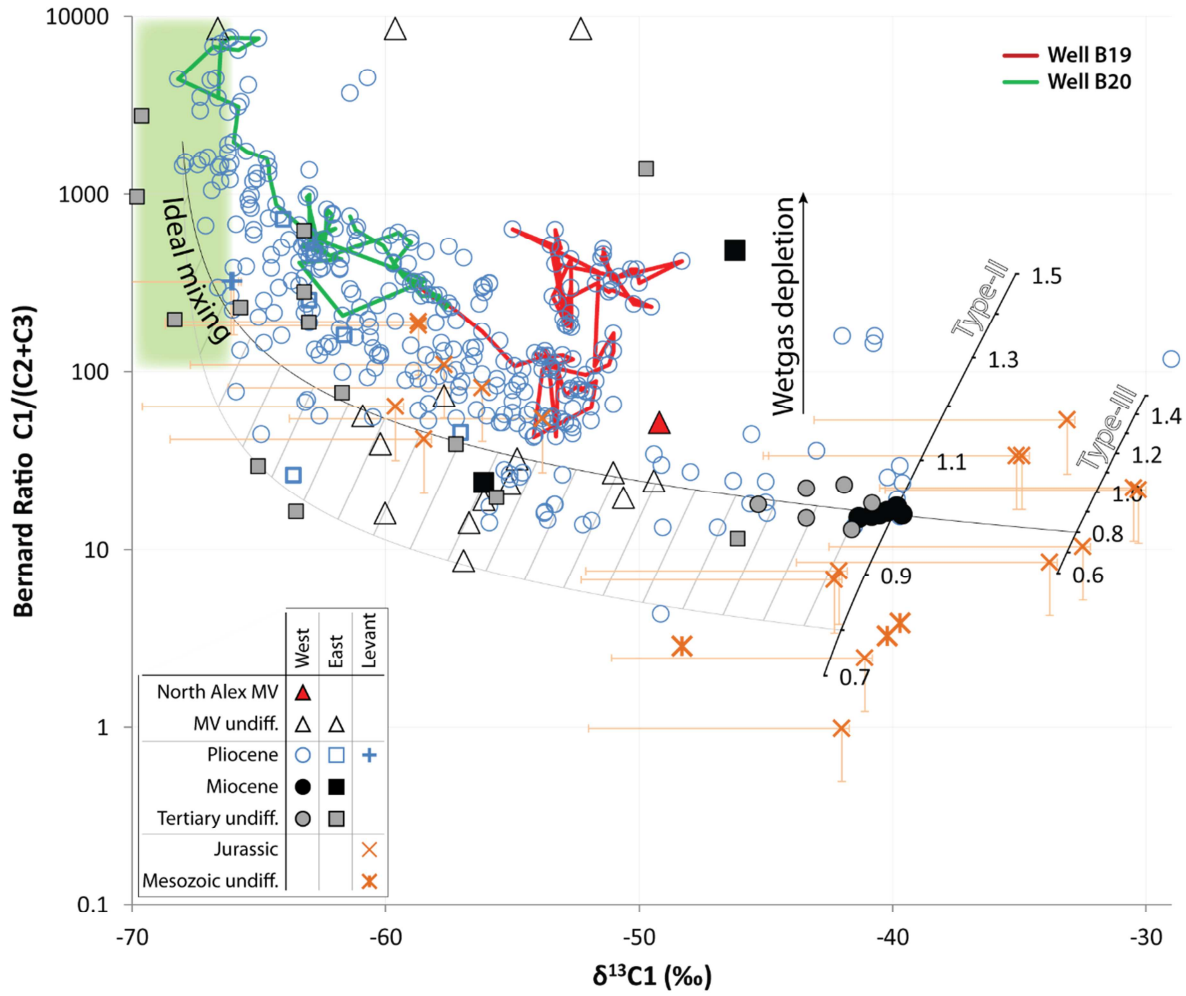

Figure 6 Bernard-type diagram with microbial end-member field (green box) and thermogenic source signals. Maturities (VR in %Ro) for type-II and type-III source rocks with $\delta^{13}C_{kerogen}$ = -26.5 ‰ are shown (Berner & Faber, 1996). It is evident that most subsurface gas samples collected in the greater Nile Delta (Figure 2) plot above the theoretical end-member mixing lines (Equation 2), indicating the preferential removal of C2+ from the system. Data in the hashed area below the ideal mixing line of the primary source composition (type-III) is captured by assuming secondary contributions of type-II source kerogen (Table 2). The transition between mixing trends in wells B19 (red line) and B20 (green line) are discussed in the section about the Horus case study.

3.3 Biodegradation of C2+ alkanes

The data in Table 1 suggest that the primary gas components least affected by biodegradation in sulphate-free environments are methane and ethane, so that the mixing of microbial and thermogenic gases is most clearly shown in the methane-ethane system (Prinzhofer & Huc, 1995). Cross-plotting the carbon isotope ratios of methane and ethane in Figure 7a shows that the thermogenic ethane fingerprint is only affected by the addition of microbial ethane if the system is already dominated by primary microbial gas (δ^{13}C1 < -60‰, equivalent to approximately x_t < 25% and $C2_t$ < 2.0%). This observation reflects the compositional difference between the two primary gas types, since thermogenic gas in this region contains up to 4.5 vol.% ethane (Table 2) compared to trace ethane concentrations in microbial gas (Oremland et al., 1988; Hinrichs et al., 2006).

By assuming that the system is dominated by primary methane we can estimate the thermogenic component $C1_t$ from the compositional analysis C1 for each gas sample using Equation 3.

Equation 3 $$C1_t\ [vol.ppm] = \mathrm{C1} * x_t$$

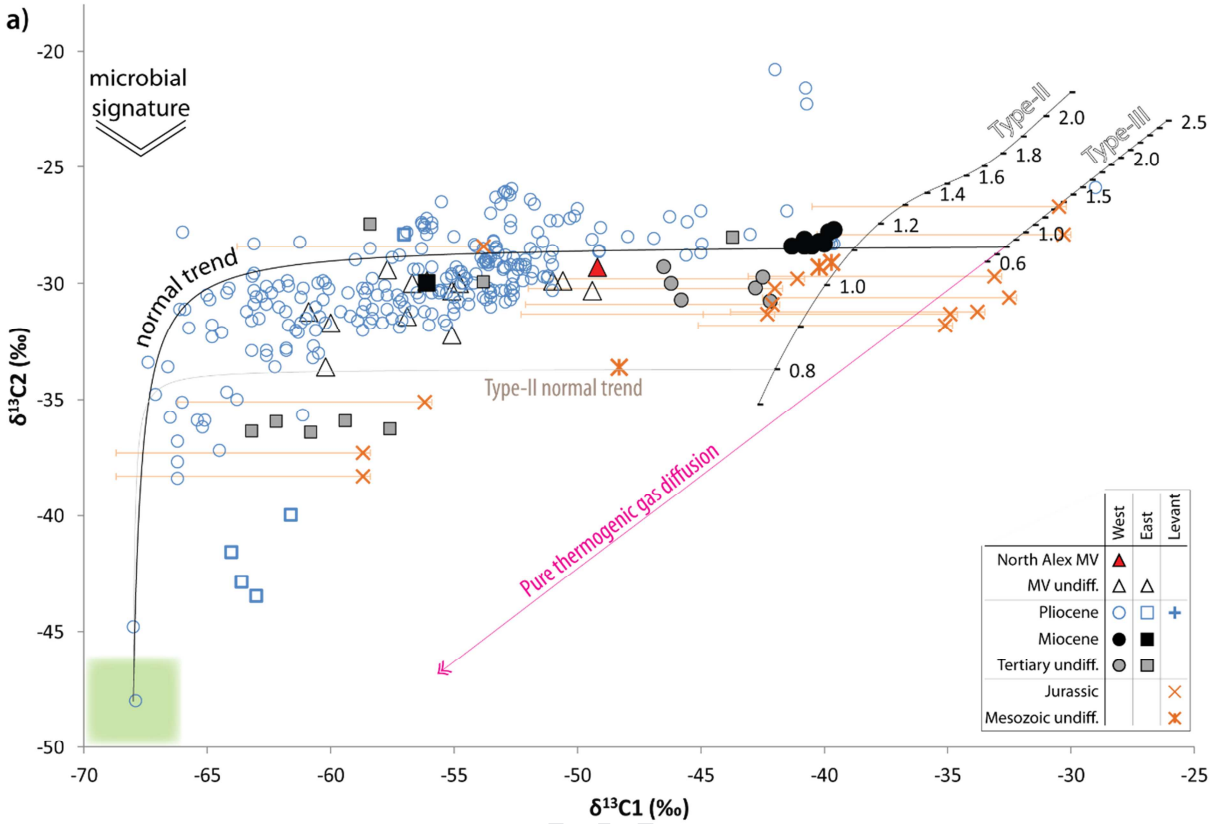

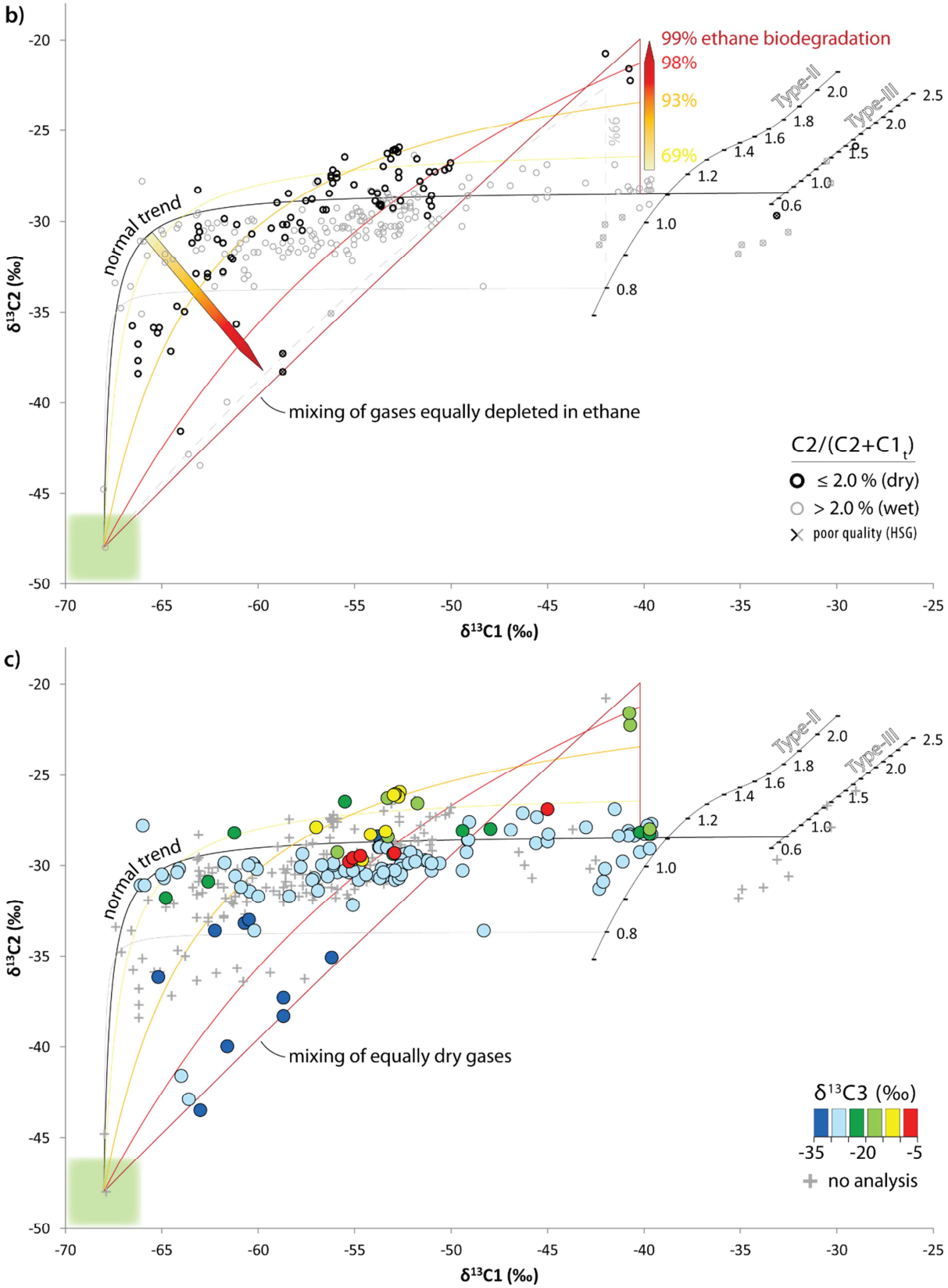

Figure 7 Mixing diagrams in the methane-ethane carbon isotope system. (a) The bulk of the dataset plots between the ideal mixing lines (labelled 'normal trend') of thermogenic gases from type-III and type-II sources. Note that many headspace gas data points from the Eastern Mediterranean (Feinstein et al., 2002) appear to follow the diffused thermogenic gas pathway (magenta line; calculated from Fick's Law for open system diffusion in semi-infinite space after Prinzhofer & Pernaton (1997, and references therein) with an effective diffusion coefficient of D=0.7 for sandstones from Schloemer & Krooss (2004)). (b) A subset of samples is particularly dry with C2/(C2+C1$_t$) ≤ 2.0%. These can be matched by open system Rayleigh fractionation modelling (Clayton 1991, and references therein) for biodegradation of the thermogenic

ethane end-member listed in Table 2. Thermogenic gases that have seen 69-99% ethane stripping become compositionally similar to the dry microbial gas (green box) so that isotope effects become sensitive to methanogenic dilution over the full methane-ethane $\delta^{13}C$ mixing interval. The effective shift of the original mixing line (normal trend) is highlighted by two arrows with a yellow-to-red colour gradient infill. Note the use of composite symbols in this figure. (c) The unaltered thermogenic $\delta^{13}C3$ signature (~ -27 ‰; light blue) follows the normal mixing trend whereas anomalously light and heavy carbon isotope signatures tend to align with the dry gas mixing lines. Microbial cycling of light alkanes in the Nile Delta Pliocene is hence controlled by the coupling of methanogenesis and alkanogenesis with biodegradation of C2+.

Since the vast majority of C2+ alkanes in the Nile Delta Pliocene derive from catagenesis (Table 1), removing the methanogenic methane component via Equation 3 allows the normalization of the C2+ concentrations relative to the thermogenic methane component. We consider $C2/(C2+C1_t)$ as a proxy for the identification of anomalies in C2+ concentration that suggest the presence of a second, steep carbon isotope mixing trend. Data in Figure 7b suggest that some gases are compositionally drier than the gas samples that plot on the main trend (black line), with $C2/(C2+C1_t) \leq 2.0\%$. We interpret the steeper trend on the $\delta^{13}C1$ vs. $\delta^{13}C2$ plot (Figure 7b) as mixing of primary microbial gas with a dry and isotopically heavy counterpart. These two end-member gases are equally depleted in ethane, so that $\delta^{13}C2$ responds to compositional change over the full length of the mixing pathway. Rayleigh fractionation modelling suggests that pristine thermogenic wet gas must see > 70% ethane biodegradation to arrive at the dryness and carbon isotope signatures that we observe in Figure 7b. We observe a similar mixing relationship between $\delta^{13}C2$ and $\delta^{13}C3$ (Figure 7c), implying that both ethane and propane were biodegraded simultaneously.

The ethane carbon isotope response to biodegradation is very subtle compared to that of biodegraded propane (Figure 8). High ethane-to-propane carbon isotope ratios are controlled by heavy $\delta^{13}C3$ in stratigraphic levels where there are free gas accumulations (Böker, 2011). All clearly biodegraded propane samples were collected at formation temperatures of 45–65°C. This window is well below the temperature limit for fermentative microbes (Grassia et al., 1996) and within the optimum 30–65°C window for methanogenic archaea (Zeikus & Winfrey, 1976; Zeikus & Wolfe, 1973). At the same time, the $\delta^{13}C2/\delta^{13}C3$ ratios plotted in Figure 8 show that gases collected from (i) regional mud volcanoes, (ii) Nile Delta Miocene reservoirs and (iii) Jurassic reservoir rocks in the Levant Basin (Figure 2) contain unaltered thermogenic wet gases.

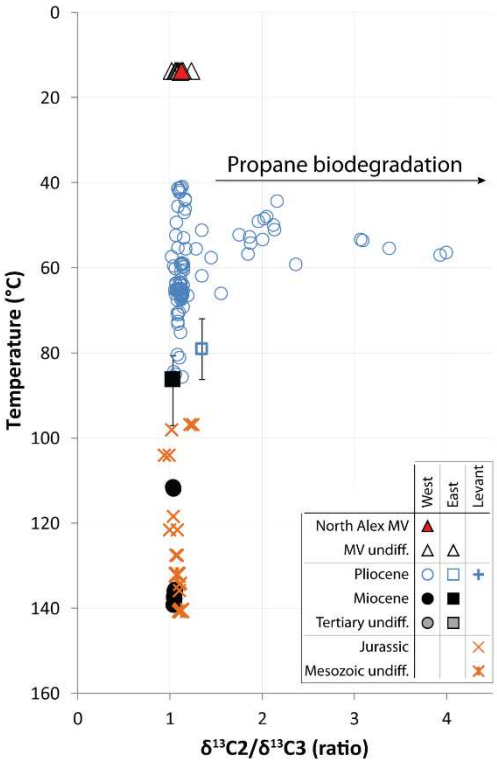

Figure 8 Distribution of ethane-to-propane carbon isotopic ratios relative to the present-day temperature of the sampled strata. High ratios, which are indicative of propane biodegradation because $\delta^{13}C3$ becomes less negative whereas $\delta^{13}C2$ remains effectively unchanged, occur at temperatures between 45-65°C. Note that the data shown represent only a subset of the samples displayed in Figure 7a due to overall low abundance of propane and thus lack of analytical data.

The offset of $\delta^{13}C2$ from the thermal maturity trends in Figure 7, and our interpretation of Figure 8, support the idea that gases which are dry and have isotopically heavy C2+ relate to biodegradation rather than to the presence of dry hydrocarbon gas from a subordinate, late-stage mature source rock from the Mesozoic. Our observations allow the general statement that in the Nile Delta, at least 70% of thermogenic ethane needs to be removed, either passively by dilution into dry microbial gases or actively by *in situ* biodegradation, before these processes cause notable carbon isotope shifts.

3.4 Methanogenic biodegradation

The carbon isotope systematics presented above suggest the presence of three hydrocarbon gas types: (i) dry and carbon isotopically light microbial gas, (ii) wet and carbon isotopically heavy thermogenic gas, and (iii) dry gas with biodegraded, carbon isotopically heavy C2+. The coupling of methanogenesis to biodegradation has been described by Jones et al. (2008) and involves closed-system methanogenic cycling of CO_2 that is supplied by microbes which biodegrade C2+ in a syntrophic microbial environment (Table 1). Since we see evidence of microbial activity in the carbon isotopic signature of both ethane and propane (Figure 7 and Figure 8), we now investigate the relationships of $\delta^{13}C2$ and $\delta^{13}C3$ with $\delta^{13}C\text{-}CO_2$. Figure 9 shows two distinct populations:

- Population 1: $\delta^{13}C2$ and $\delta^{13}C3$ remain relatively unchanged with increasing $\delta^{13}C\text{-}CO_2$; C2 tends to be 1-2‰ heavier at the most positive $\delta^{13}C\text{-}CO_2$ values.
- Population 2: heavy $\delta^{13}C3$ tends to be associated with heavy $\delta^{13}C\text{-}CO_2$

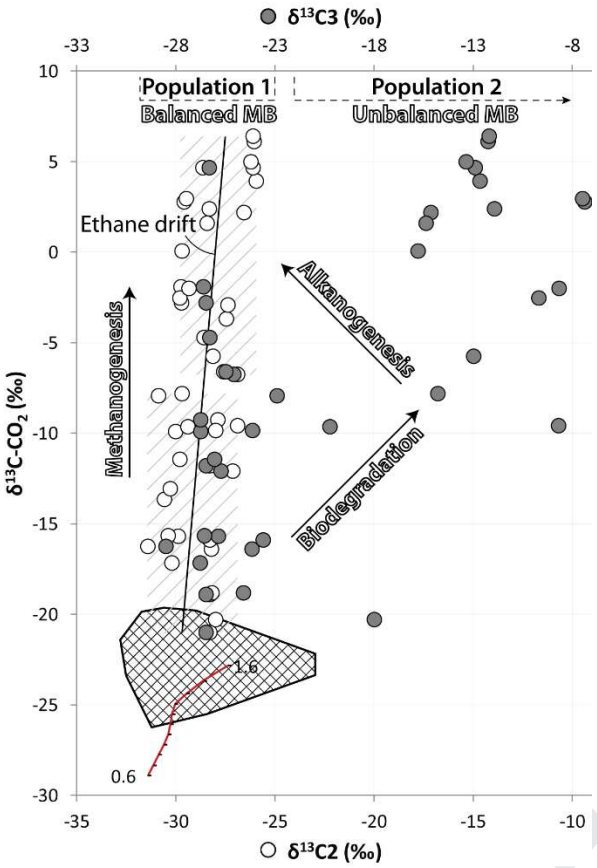

Figure 9 Relation between the carbon isotopic compositions of ethane/propane and CO_2. The solid red line denotes the maturity trend of thermogenic gas generation in a semi-open system in the vitrinite reflectance range from 0.6 to 1.6 %Ro (Takahashi & Suzuki, 2017). The cross-hashed field is the pyrolysis data envelope discussed in Section 3.1. See text for discussion.

The majority of CO_2 (and C1, not shown) carbon isotope signatures belong to Population 1. The shift to higher $\delta^{13}C$-CO_2 supports the idea that hydrogenotrophic methanogenesis is the dominant microbial process (Table 1) while ethane and propane are microbially cycled, i.e. both generated (alkanogenesis) and destroyed (biodegradation), leading to an approximate net-zero effect in their carbon isotope ratios derived from their thermogenic source (Table 2; Böker, 2011).

Population 2 was found to exclusively occur in hydrocarbon accumulations where gas saturations are high (Böker, 2011). In this case, gases that have been biodegraded in the presence of connected pore water (Röling et al., 2003), for example near the gas-water contact, become inaccessible to any further microbial cycling subsequent to advection or diffusion up into the gas column (Kieft et al., 1993; Tyler et al., 1994; Grant & Whiticar, 2002). The signature of biodegraded gases formed in the gas-water transition zone is thus preserved through upwards migration into the hydrocarbon column (Head et al., 2003). Preservation of Population 2 in Figure 9 is indicative of situations where biodegradation rates outpace the combined supply of ^{12}C-rich wet gases through (i) thermogenic charge and (ii) *in situ* alkanogenesis. The latter involves ethanogenesis and propanogenesis (Table 1) from acetoclastic microbial synthesis (Hinrichs et al., 2006), a metabolic pathway that accompanies syntrophic methanogenic biodegradation (Jones et al., 2008).

Population 1 can be described as balanced or regular methanogenic biodegradation (MB), indicative of an open system environment where all microbial activity occurs simultaneously and at similar rates, whereas Population 2 indicates unbalanced MB with a dominant biodegradation footprint in a closed or partially closed system. The latter is only fully observed in propane data (Population 2). Ethane does not appear as severely unbalanced as propane, supported by field observations that ethanogenesis has a faster metabolic turnover compared to propanogenesis (Table 1). However, the

slight drift in $\delta^{13}C2$ (open circles, trendline through hashed areas in Figure 9) to more positive values with an increase in $\delta^{13}C\text{-}CO_2$ suggests that methanogenesis may indeed be accompanied by a subtle carbon isotopic expression of ethane biodegradation.

Our data suggest that the carbon isotope ratios of ethane and propane are preserved in gas accumulations where gas saturations are high, so that biodegradation footprints are indicative of a trapped gas phase with little water. Although the carbon isotopic signature of propane is particularly sensitive to biodegradation (James & Burns, 1984; Kinnaman et al., 2007) as shown by the high $\delta^{13}C2/\delta^{13}C3$ ratios in Figure 8, ethane is typically more abundant in natural gas systems (Table 1) and thus generally provides a more comprehensive analytical dataset. Consequently, we propose that the subtle carbon isotope response of ethane biodegradation shown in Figure 7 and Figure 9 may offer a way of quantifying the mixing history of biodegraded gases in an aqueous, methanogenic environment. The carbon isotopic composition of methane is not significantly affected by secondary alteration, so that $\delta^{13}C1$ can be tentatively used to quantify the relative proportions of mixed thermogenic and hydrogenotrophic gases (Equation 1).

4 Case studies

In this section we use our conclusions on the controls of gas geochemistry to interpret the processes which govern the occurrence, migration and chemical signature of gases in four wells drilled through mud-sand sequences in the Western Nile Delta fan. The wells are clustered into two case studies: B19 and B20 to the north-east and south-east of the Horus mud volcano; B22 and B24 to the north and west of the North Alex mud volcano (Figure 10). Water depths range from 350m to 650m and pore pressures above and below the Pliocene gas zones are hydrostatic. Isotube sampling starts in Pliocene strata at around 500m below mudline and continues to about 1350m in B19, 1800m in B20 and B24, and 2000m in B22. The average sampling step for these four borehole sections varies between 7m and 11m and samples were taken from both the mud-rich and sand-rich sections; the data comprises a total of 582 gas samples, of which 251 have isotope values that pass the quality control in Section 2.

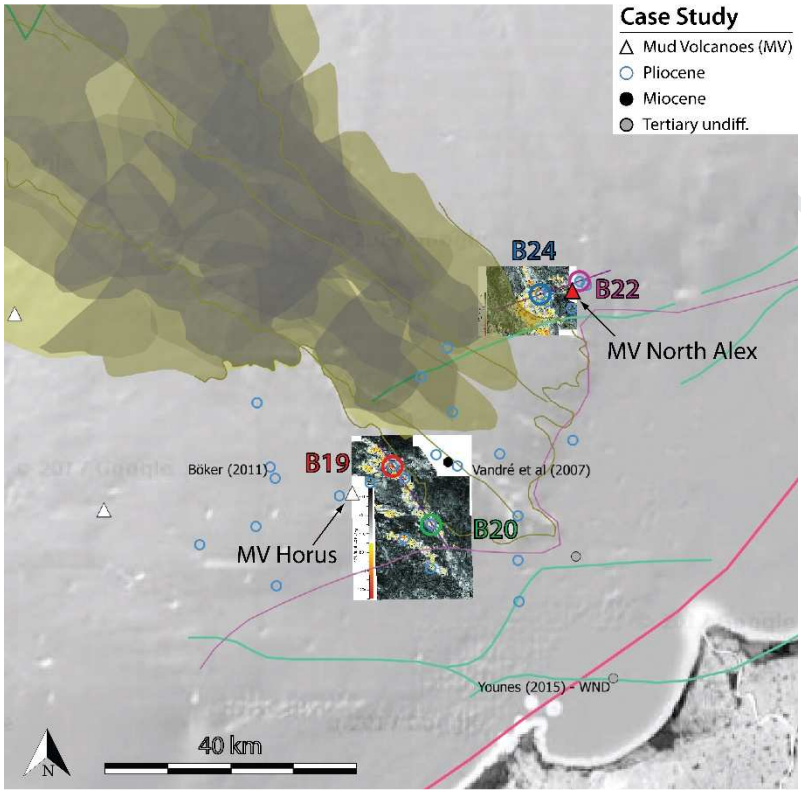

Figure 10 Location of Horus and North Alex study areas between the present-day shelf edge (pink line) and slope failure deposits (brown fields) of the Rosetta channel branch (Loncke et al., 2008). See Figure 2 for full legend. Detailed RMS amplitude maps are shown in Figure 11 and Figure 16. Satellite imagery courtesy of Google.

4.1 Horus area

The slope channel reservoir of the Horus case study is dissected by a normal fault that separates the commercial gas accumulation at B19 from the non-commercial, south-eastern branch drilled by B20 (Figure 11).

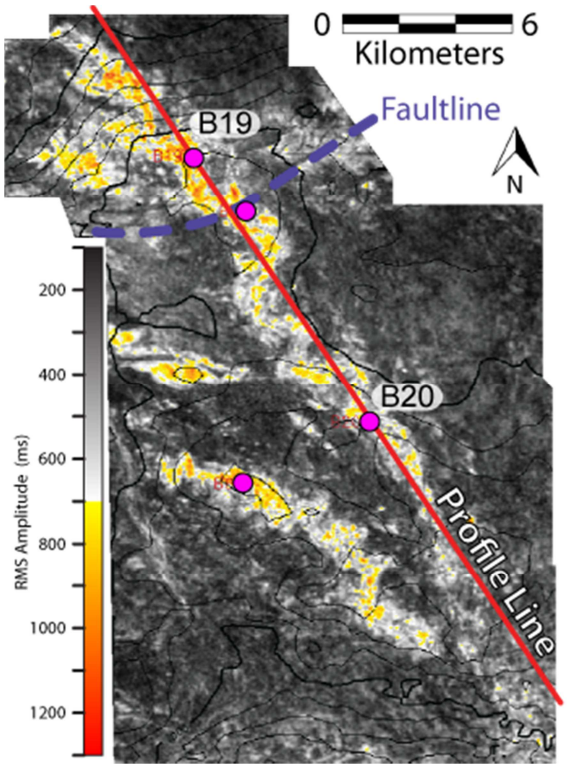

Figure 11 RMS amplitude map of channel reservoirs in the Horus case study. The brighter colours indicate elevated seismic amplitudes in sand-rich areas and pink circles represent well penetrations. Note the normal fault that compartmentalises the north-western branch with well B19 from the south-eastern branch with well B20. The axial cross-section is shown in Figure 15. Modified after Böker (2011).

Sands within Well B19 in the north-western part of the channel complex hold a gas column of 230m whereas the sands within B20 to the south-east contain no more than 25m gas at low gas saturations. The trap configuration has a mudstone top and base seal plus mudstone as three of the lateral seals. A fault seal provides the lateral seal on the SW flank of the accumulation drilled by B19 (Figure 11). The sealing character of the fault between B19 and B20 is indicated by very poor pressure communication between the two boreholes, as determined by pump tests (DST). The regional top seal in this area is dominated by heterogeneous turbidite/levee and mass transport deposits with intermittent hemipelagites. Core images from the top seal at B20 show small-scale sandstone intrusions at multiple stratigraphic levels (Figure 12). Questions that arise from this scenario are whether B20 has lost its gas through the seal or has never received charge, and whether gas within the main sandstone package at B19 has leaked into the caprock.

Figure 12 Selection of core photographs that show sandstone intrusions into the mudstone caprock of well B20 of (a-b) vertical break-through and (c-d) fracture-associated types. Depth in metres below mudline. See Figure 14 for stratigraphic context.

4.1.1 Gas profile of Well B19

In the mud-rich sequences both above and below the channel reservoir sand, the isotopic composition of methane is consistently between -55 and -50‰, declining at the base of the well to -58‰ (Figure 13). These data indicate a consistent mix of thermogenic and microbial methane (x_t ~ 50%, Equation 1). In the sandstone reservoir, $\delta^{13}C1$ is constant through the highly gas-saturated zone but is 4‰ lighter than the methane in both the top seal and underseal.

In the sandstone reservoir, both C3 and CO_2 are isotopically heavier than in the underlying mud-rich unit, indicating an unbalanced methanogenic biodegradation (MB) footprint within the gas accumulation (see Figure 9). C2 in the sandstone reservoir also shows elevated $\delta^{13}C$ values compared to C2 in the mud-rich units; here, gases are sufficiently dry (($C2/(C2+C1_t)$ < 2.0%; Figure 7) that ethane biodegradation is evident in the carbon isotope ratio. We conclude that MB in the B19 channel sandstone is likely to be occurring *in situ* and at rates that outpace thermogenic charge.

Gases in the deeper, mud-rich section between ca. 1150m and 1300m are relatively rich in thermogenic C2+, obscuring any response of $\delta^{13}C2$ to MB, which is nevertheless evident from the heavy $\delta^{13}C3$ and $\delta^{13}C$-CO_2 signatures. This mud-rich section was either charged more recently than the dry gas reservoir above or MB is less effective at these slightly higher temperatures. At the base, $\delta^{13}C1$ becomes lighter and shifts toward the burial trend displayed in Figure 5 while transitioning into the mixing trend of gases sampled in well B20 (Figure 6).

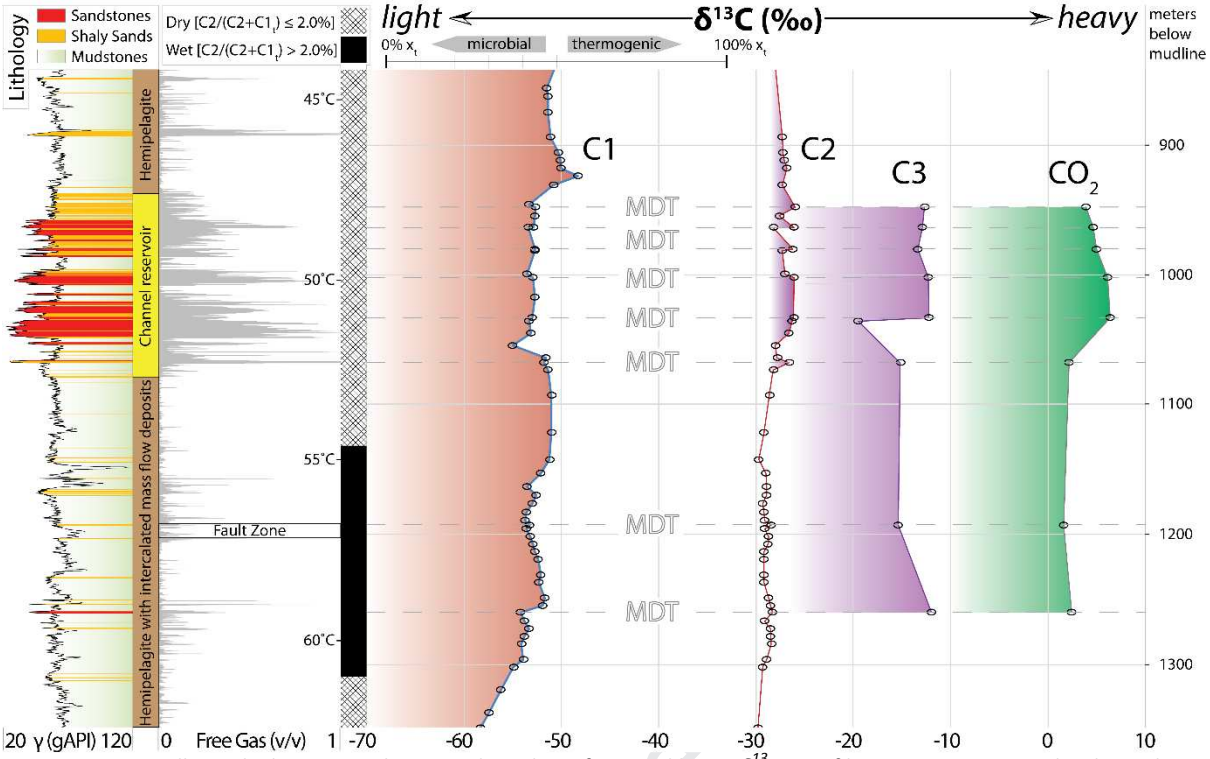

Figure 13 B19 well panel. The section shows a relatively uniform and heavy $\delta^{13}C1$ profile. Gas signatures in the channel reservoir exhibit unbalanced MB (heavy $\delta^{13}C3$ and $\delta^{13}C\text{-}CO_2$). Here, ethane appears to respond to biodegradation as $\delta^{13}C2$ is 2-3‰ heavier than expected from the pristine thermogenic fingerprint (discussed in the text). In the deep section, from ca. 1150m and 1300m, higher concentration of C2+ obscure any response of $\delta^{13}C2$ to methanogenic biodegradation, indicating that either charge is more recent than in the reservoir zone and/or reflecting subdued metabolic turnover at elevated temperatures. Note that the fault crossing at 1200m is sub-seismic scale. "Free Gas" is the hydrocarbon saturation from wireline log analysis.

4.1.2 Gas profile of Well B20

Gas isotope profiles in Well B20 are radically different to those in B19. Figure 14 shows that in B20, gases are exceptionally dry throughout the entire section; $\delta^{13}C1$ increases steadily from -66‰ (x_t ~ 5%, Equation 1) in the mud-rich section at 1050m to -58‰ (x_t ~ 25%) at 1700m in the mud-rich section below the channel sandstone. Below 1700m, $\delta^{13}C1$ decreases slightly to -61‰.

The gas is dominated by microbial methane and the main isotope trend is consistent with generation from organic matter (Figure 5). With continuing microbial generation, where the isotopically light methane is progressively extracted, the organic matter is becoming isotopically heavier with ongoing burial/time. The steady trend to isotopically heavier methane suggests that the earlier formed, isotopically lighter methane may have been continuously expelled from the mud-rich sections. However, $\delta^{13}C1$ is slightly heavier than values expected for pure microbial methane (Figure 5 and Figure 6), suggesting a small addition of thermogenic gas throughout the section. This is also seen within the channel sandstone complex, where one sample from a sand with the highest gas saturation at around 1430m (based on wireline log data), contains a minor thermogenic component with $\delta^{13}C1$ elevated by +5 ‰ from the background. $\delta^{13}C2$ is consistently around -30 ‰ in both channel sands and underlying muds, slightly lighter than the regional thermogenic $\delta^{13}C2$ (-28.5 ‰; Table 2) and potentially indicating a small but persistent alkanogenic contribution.

Biodegradation cannot be observed (see $\delta^{13}C3$) due to the low concentrations of thermogenic wet gases. And, although the residual gas in the system has near-methanogenic $\delta^{13}C1$, the isotopic composition of CO_2 suggests that metabolic rates are low compared to the MB activity documented in well B19.

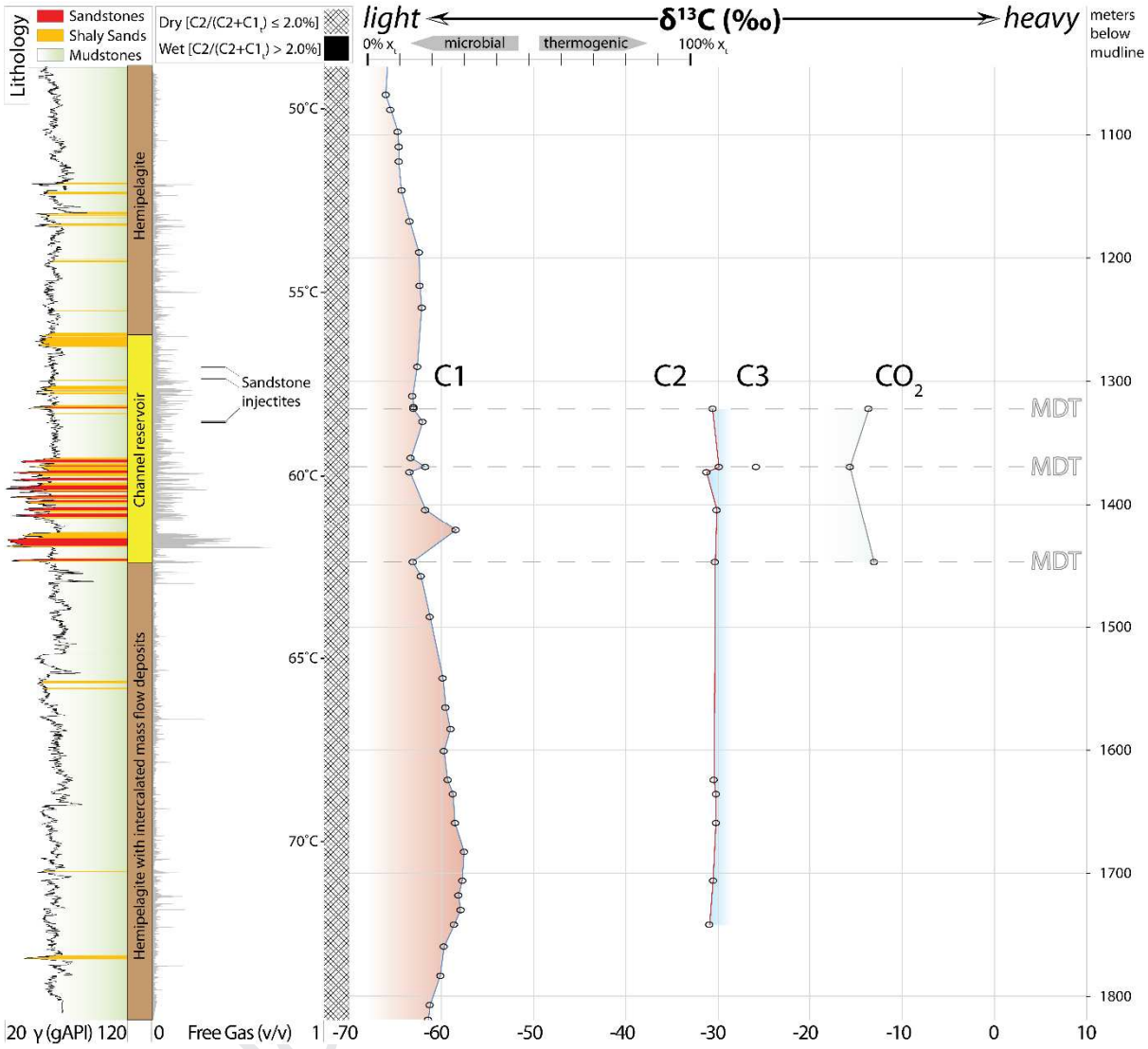

Figure 14 B20 well panel. Methane has a microbial (light) $\delta^{13}C1$ signature that runs parallel to the burial trend in Figure 5. C2+ concentrations are below 2%, $\delta^{13}C\text{-}CO_2$ signature is not controlled by methanogenesis, and $\delta^{13}C2$ is 1-2‰ lighter than the regular thermogenic fingerprint, suggesting some degree of alkanogenic microbial activity. The remnant thermogenic imprint together with sub-commercial gas saturations in the channel and presence of sandstone injectites in the top seal (Figure 12) imply that gases have migrated into the upper mud-rich sections. "Free Gas" is the hydrocarbon saturation from wireline log analysis.

4.1.3 Migration in the Horus area

In B19, $\delta^{13}C1$ sampled within the top seal is more enriched in ^{13}C than in the reservoir below. Gas in the reservoir contains a higher proportion of microbially-generated gas, shifting the bulk signature of $\delta^{13}C1$ by -4‰. This may represent microbial gas which has accumulated in the sandstone during its burial, to which thermogenic gas has been added through lateral charge along dipping sands (Figure 15). Additionally, values of $\delta^{13}C3$ and $\delta^{13}C\text{-}CO_2$ in the reservoir gas indicate that the rate of thermogenic charge is outpaced or matched by the rates of methanogenic biodegradation (Aitken et al., 2004; Jørgensen & D'Hondt, 2006). The greater, constant proportion of thermogenic gas in the mud-rich sections both above and below the channel sandstone, suggests that migration has occurred laterally through thin silts and sands in the mud-rich sections, and then vertically at the structural high drilled by Well B19 (Figure 15).

Our data do not resolve whether mixing of thermogenic and methanogenic gas has occurred *in situ* or elsewhere, earlier on the migration pathway, and we cannot directly discriminate between the

relative contributions of lateral versus vertical gas flux in the mud-rich sections above and below the main sandstone. However, given the structural setting shown in Figure 15, we expect that a combination of a sealing fault on the lee side of the well and/or structural focus at B19 resulted in the accumulation of laterally migrating thermogenic or mixed thermogenic-microbial gases. This would increase the gas saturations in higher permeability, lower capillary entry pressure thin beds and hence increase the probability of establishing sub-vertical, gas-filled percolation networks (Carruthers & Ringrose, 1998). Continued lateral migration to the location of B19 (Figure 15) was prevented either by a lack of charge and/or the vertical leakage of gas at the structural high. We will elaborate on the potential migration mechanisms in the discussion.

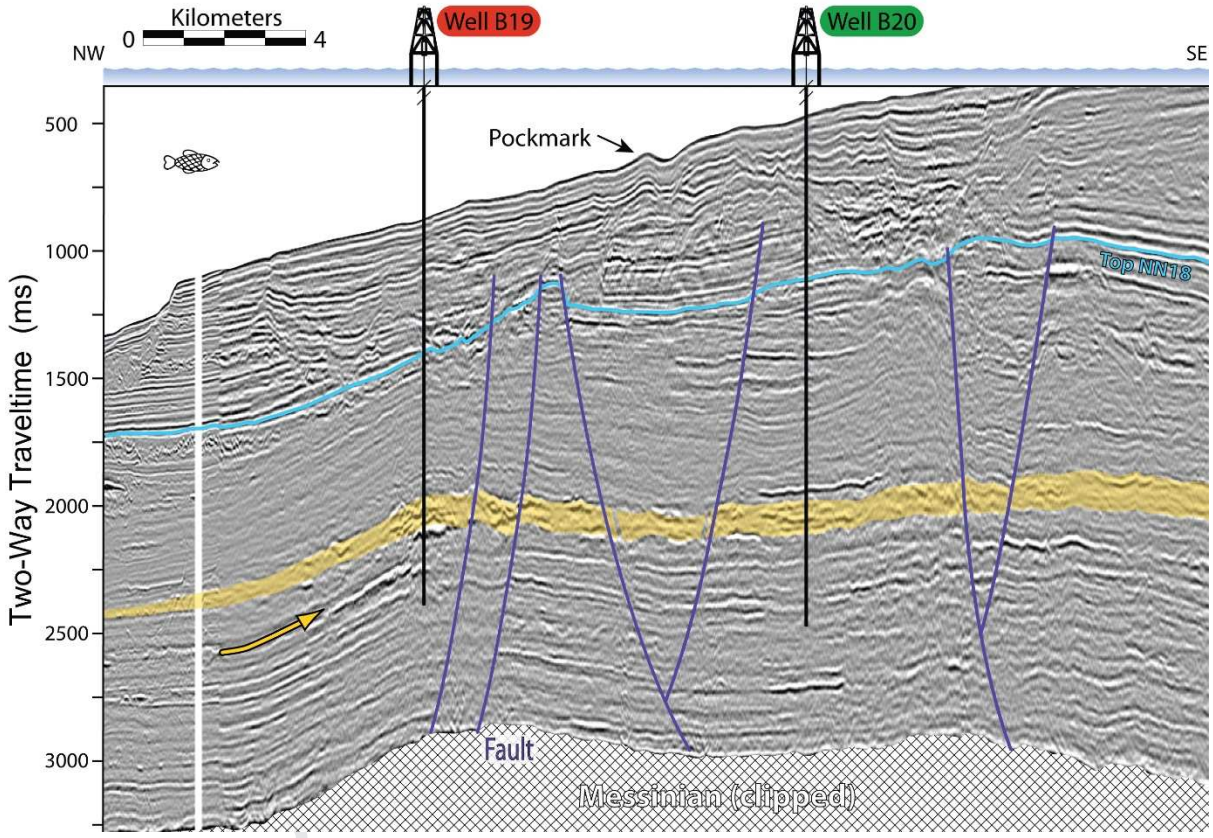

Figure 15 Seismic section parallel to the channel axis of the Horus case study shown in Figure 11. The NN18 maximum flooding surface (pale blue) is situated near the Plio-/Pleistocene stratigraphic boundary (Figure 1). The sealing character of the faults is supported by the presence of a thermogenic gas accumulation in the B19 channel branch (shaded yellow) whereas the B20 branch to the south-east has a low saturation of mainly methanogenic gas. The thermogenic charge in B19 is suggested to migrate foremost updip from the basin centre in the north-west (orange arrow). Modified after Böker (2011).

4.2 North Alex area

In the North Alex area, B24 targeted a channel-levee complex whereas the main objective of B22 was a shallower levee reservoir that transitions laterally to an adjacent channel further east (Figure 16).

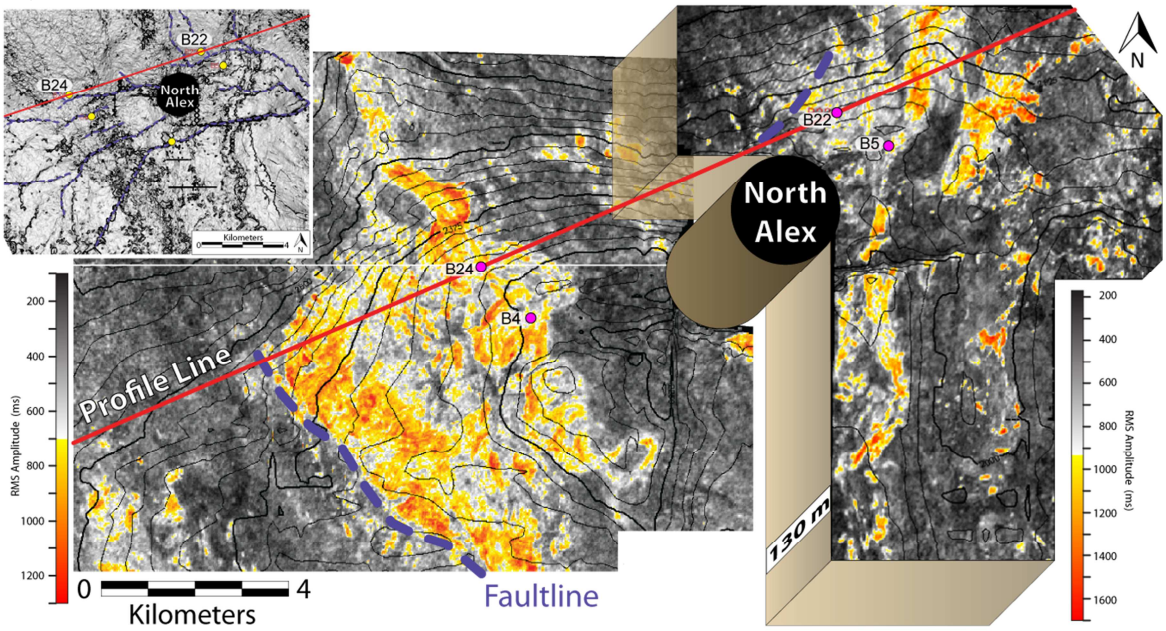

Figure 16 RMS amplitude composite map of the North Alex case study. The brighter colours indicate elevated seismic amplitudes in sand-rich areas. The cylinder marks the perimeter of disturbed strata around the mud volcano. B24 penetrates a channel adjacent to a fault-bounded levee complex. The shallow reservoir in B22 is a channel-associated levee deposit. The profile line corresponds to the cross-section displayed in Figure 19. Note the WSW-ENE striking fault swarm shown in the seismic similarity map inlet. Modified after Böker (2011).

Gas column heights are 240m in the B24 reservoir and 100m in the main (shallow) reservoir in Well B22. The caprock at B22 is dominated by turbidite/levee deposits whereas the B24 reservoir is situated at the base of a stacked channel sequence within a series of levee, mass transport deposits, and hemipelagites. Although the two wells produce gas from different reservoirs at different stratigraphic levels, both are (i) marginally confined by a normal fault and (ii) proximal to the North Alex mud volcano.

4.2.1 Gas profile of Well B22

At the base of the well at *ca*. 2000m, gas is almost purely microbial. Up through the channel levee system, to 1720m, the proportion of thermogenic gas in the thermogenic-microbial mix generally increases. Gas from 1720m to 1580m is compositionally very similar, with C1 indicating a mixture of microbial and thermogenic gas but with C2+ which is unaffected by biodegradation. Carbon isotope ratios of CO_2 are governed by hydrogenotrophic methanogenesis as they are up to 18‰ heavier than the range of isotopic compositions of pristine thermogenic gases shown in Figure 9. Despite the methanogenic imprint in $\delta^{13}C$-CO_2, gases in this interval are relatively wet, have thermogenic C2 and C3 fingerprints, and contain up to 50% thermogenic methane (Table 2, Figure 7). These data suggest that the rate of gas charge is greater than the rate of microbial metabolism.

From 1580m to 1350m, through the mud-rich section comprising hemipelagites and mass flow deposits, the proportion of thermogenic gas gradually decreases to zero, before increasing steadily from 1350m up to the levee at 1150m (Figure 17). Exceptionally light $\delta^{13}C2$ indicates that the inter-reservoir zone has received very little thermogenic charge and that the gas composition is dominated by *in situ* methanogenic and alkanogenic synthesis.

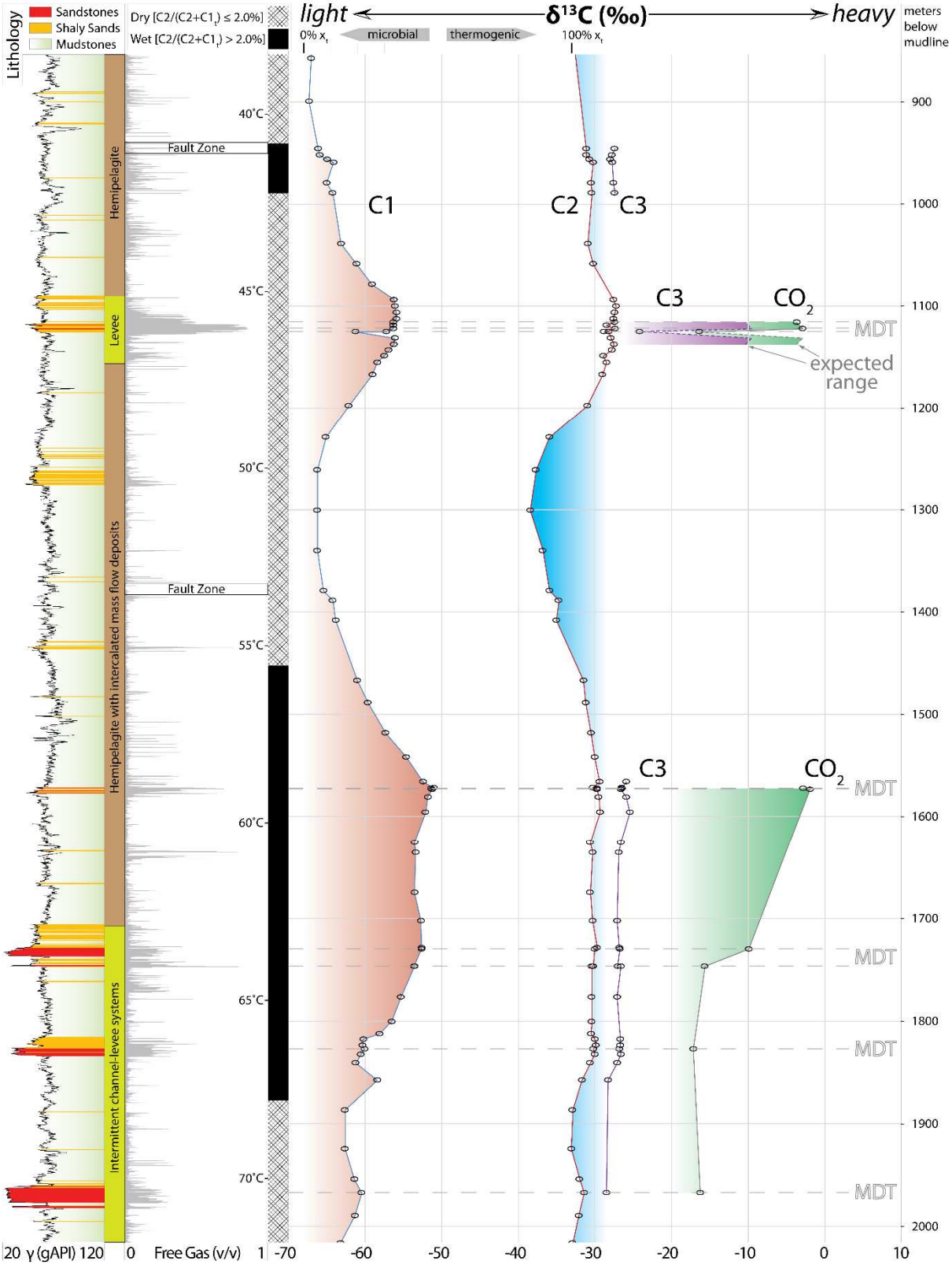

Figure 17 B22 well panel. Methane and – to a lesser degree – ethane carbon isotope profiles exhibit a low amplitude curvature with strong thermogenic fingerprint across the upper (levee) and most of the lower reservoir zones. Note the difference in dryness: relatively wet gas in the lower reservoir obscures a δ^{13}C2 response to microbial cycling while δ^{13}C3 and δ^{13}C-CO_2 indicate balanced methanogenic biodegradation; the levee reservoir gas is biodegraded to the extent that only MDT downhole sampling methods recovered enough C3 for isotope analysis (unbalanced methanogenic biodegradation). The strong alkanogenic (light) δ^{13}C2 signature in the inter-reservoir zone indicates an effective barrier to fluid exchange at the base of this section (see text for detailed discussion). "Free Gas" is the hydrocarbon saturation from wireline log analysis.

The levee reservoir at 1090-1150m contains a mixture of thermogenic and microbial gas. The absence of C3(+), limited CO_2 and the overall dryness of the gas suggest that C3+ hydrocarbons have been reduced to very low concentrations by biodegradation and that most CO_2 has been metabolized by methanogenesis. Compared to the wetter gases in the deeper channel levee zone, these gases exhibit slightly more positive $\delta^{13}C2$ (biodegradation) and more negative $\delta^{13}C1$ (methanogenesis), both supporting the presence of secondary microbial gas from methanogenic biodegradation (Table 1). The greater extent of biodegradation suggests that the rate of thermogenic charge is low compared to the rate of biodegradation. One out of the three MDT samples in this zone captured enough C3 for carbon isotope analysis. This sample was taken in a mudstone below the high saturation zone and it is not considered representative for the section, as both $\delta^{13}C1$ and $\delta^{13}C\text{-}CO_2$ are significantly lighter than their two equivalents from MDT sampling of the shallow reservoir. In Figure 17, we have scaled $\delta^{13}C3$ relative to $\delta^{13}C\text{-}CO_2$ to approximate the heavy $\delta^{13}C$ footprint that we would expect in the shallow reservoir if C3 was not biodegraded to concentrations that fall below the analytical detection limit.

Above the levee, at depths shallower than 1090m, the proportion of thermogenic gas decreases gradually up to 900m, where the gas is purely microbial. Between 940m and 990m, close to a fault zone, gases are slightly wetter and the isotopic compositions of C2 and C3 show little evidence of biodegradation, implying recent and/or relatively rapid charge that could be conducted along the fault.

4.2.2 Gas profile of Well B24

B24 drilled two reservoir zones within channel and channel-levee deposits, both containing around 40% thermogenic methane (Figure 18). In contrast to B22, gases are wet throughout the drilled section, in both the sandier and muddier intervals. The high C2 content buffers the response of $\delta^{13}C2$ to microbial degradation (Figure 7), but methanogenic biodegradation is evident in the isotopic composition of both C3 and CO_2 in gases sampled in the shallower reservoir from 1300-1450m. Gas within the deeper reservoir (1680-1730m) also shows indications of methanogenic activity ($\delta^{13}C\text{-}CO_2$ = -7‰), whereas C3 clearly has an unaltered thermogenic isotope character (balanced MB, see Figure 9), indicating that the biodegradation signature commonly observed in $\delta^{13}C3$ is obscured by thermogenic charge and – in the elevated water saturation of the surrounding mudstones – by concurrent alkanogenesis.

The compositional profiles of gas through the well section show strong similarities to those in B22. At the base of the well (1795-1730m), up through the channel-levee system, the proportion of thermogenic gas increases and there is a single sample with a near-thermogenic signal of about -42‰ (x_t ~ 70%, Equation 1). Above the channel-levee, through the mud-rich section containing hemipelagites and mass flow deposits, the proportion of thermogenic methane first decreases and then increases into the upper channel reservoir; at the same time, C2 shows a purely thermogenic signal. In the shallow channel reservoir, both $\delta^{13}C1$ and $\delta^{13}C2$ are spiky, with a second sample showing near-thermogenic $\delta^{13}C1$ at -45‰ (x_t ~ 65%). Above the channel reservoir at 1300m, the proportion of thermogenic gas decreases steadily, reaching a background value of microbial gas at around 1220m.

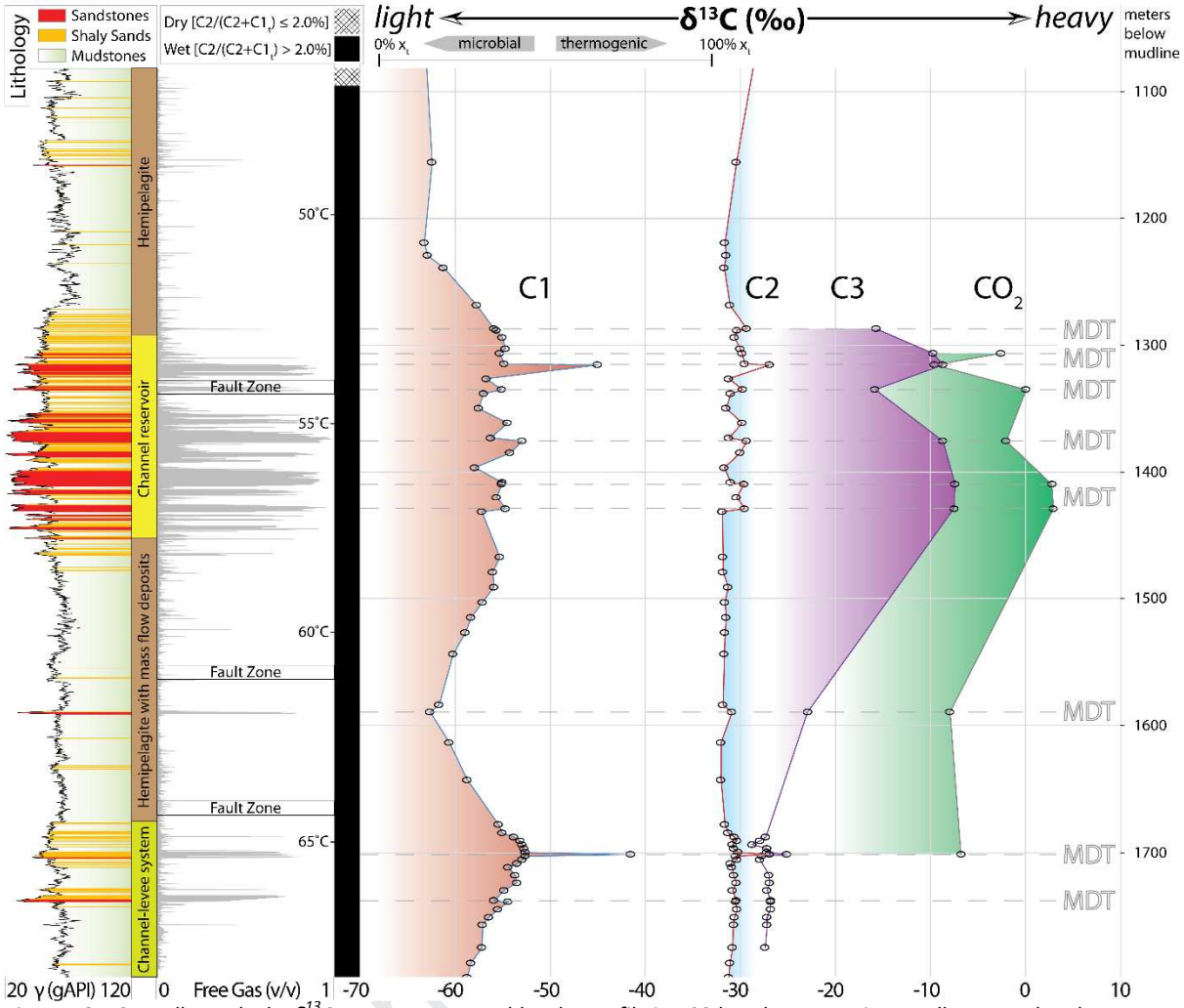

Figure 18 B24 well panel. The δ^{13}C1 curvature resembles the profile in B22 but the system is overall wetter, thereby buffering δ^{13}C2 response to microbial cycling, and isotope excursions are less pronounced. Unbalanced methanogenic biodegradation is evident in heavy δ^{13}C3 and δ^{13}C-CO_2 across the upper reservoir. The thermogenic δ^{13}C3 fingerprint in the lower reservoir suggests thermogenic charge of relatively unaltered wet gases while elevated δ^{13}C-CO_2 point toward balanced methanogenic biodegradation activity (Figure 9). MDT downhole samples in both upper and lower reservoir zones support ongoing advective injection of thermogenic gas. "Free Gas" is the hydrocarbon saturation from wireline log analysis.

4.2.3 Migration in the North Alex area

The distribution of genetic gases in the North Alex wells is entirely different from the Horus area. The relative proportions of thermogenic gases are greatest in the more permeable, sand-rich sections, with the highest proportions of microbial gas in the central parts of the mud-rich intervals, furthest from the sandstone reservoirs (Figure 17 and Figure 18). The relatively wet nature of the gas in the deep reservoir of B22 (Figure 17) and throughout B24 (Figure 18) suggests recent or ongoing charging of thermogenic gas in this area, such that the rate of charge is outstripping the rate of C2+ biodegradation. In contrast, the ultra-heavy δ^{13}C2 in the shallow B22 reservoir implies that thermogenic charge is not active at this stratigraphic level, and that C2+ gases have been biodegraded to very low volumes.

Strikingly, the ultra-light δ^{13}C2 signature in the mud-rich inter-reservoir section in B22 shows that gas is purely microbial, evidencing both methanogenesis and ethanogenesis. More generally, the

occurrence of purely microbial gas in the central parts of the mud-rich sections between the more sand-rich, channel levee systems suggests that vertical migration through these mud-rich sections is limited. Although the occurrence of thermogenic gas above the sand-rich sections does suggest some intrusion of the mud-rich top seals the steep gradient of $\delta^{13}C2$ confirms that metabolic rates outpace thermogenic charge and leakage through these mud-rich units. This type of signature where reservoirs on a single structure are separated by mudstones with an elevated microbial component is commonly observed in the Nile Delta Pliocene. We will elaborate on potential migration mechanisms and pathways in the discussion.

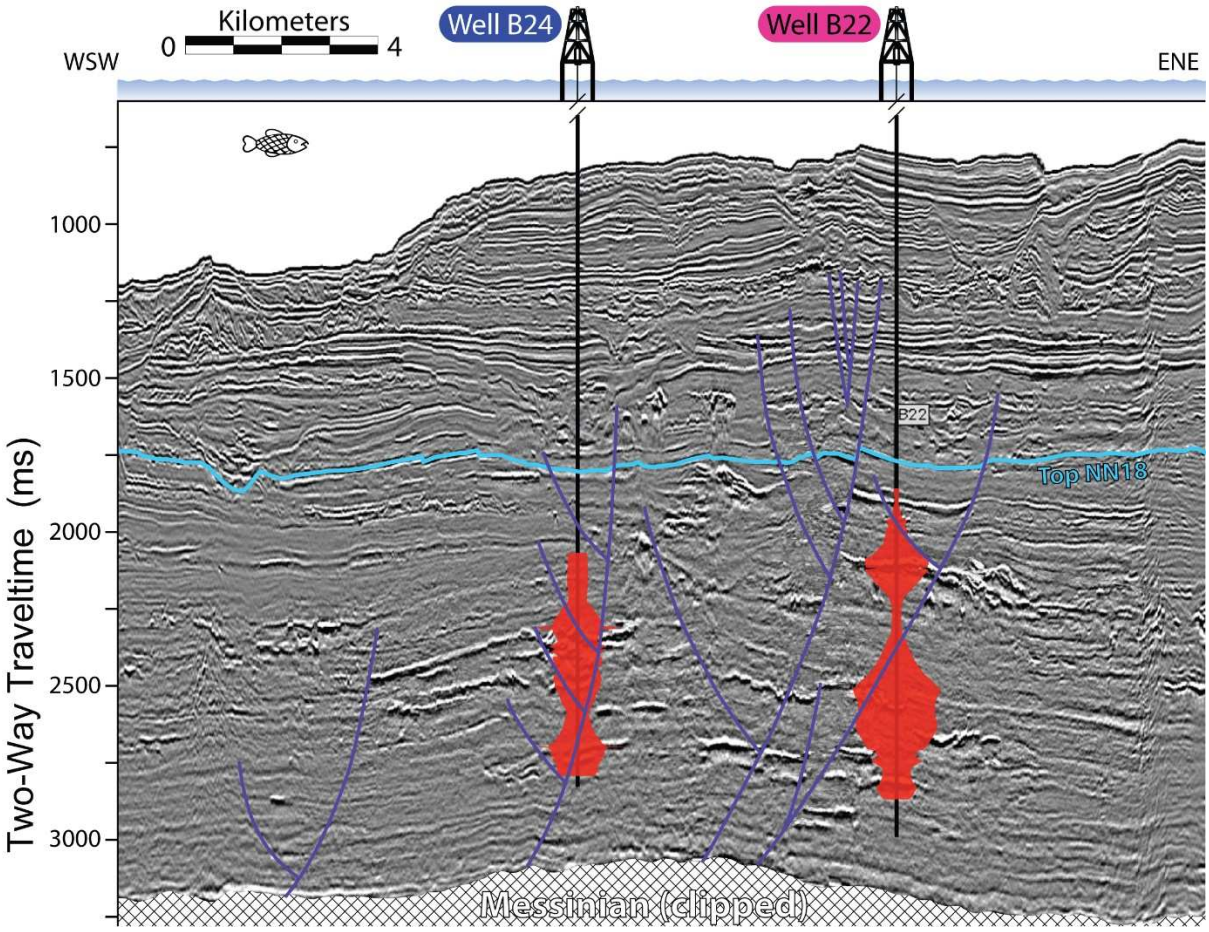

Figure 19 North Alex cross-section. B24 (left) and B22 (right) with schematic display of the potential thermogenic methane fraction (red fields mirrored on wellpaths, see $\delta^{13}C1$ profiles in Figure 17 and Figure 18 for scale). Top NN18 marks the Plio-/Pleistocene stratigraphic boundary (Figure 1). See Figure 16 for profile location and text for detailed discussion. Modified after Böker (2011).

5 Discussion

5.1 Sources and microbial alteration of gases

Careful interpretation of the methane and ethane carbon isotope dataset (Figure 6 and Figure 7) broadly confirms previous studies that suggested that the main source of thermogenic gas is type-III kerogen (Kamel et al., 1998; Sharaf, 2003; El Nady, 2007; Vandré et al., 2007; Keshta et al., 2012; Villinski, 2013; Khaled et al., 2014) with maturities around VR = 0.8 %Ro (El Diasty & Moldowan, 2013). Burial history reconstruction of organic matter maturation trends, calibrated against measured vitrinite reflectance data from the Western Nile Delta (Vandré et al., 2007), supports an Oligocene source. The scatter in Figure 6 and Figure 7 can be largely explained by assuming a secondary type-II source kerogen, which may reflect some marine influence in the Lower Oligocene (Villinski, 2013) and possibly Mesozoic source rocks of higher maturity (Sharaf, 2003; Feinstein et al., 2002; Al-Balushi et al., 2016). The combined evidence of lower maturity type-III and possibly higher maturity type-II sources is consistent with the presence of light oil and condensates in the Nile Delta petroleum province (Sharaf, 2003; El Nady, 2007; Keshta et al., 2012).

Gases sampled within the Miocene section contain at least 20% methanogenic gas (Figure 6 and Figure 7) of primary and possibly some secondary microbial origin, despite the fact that microbial life is not sustained at these elevated temperatures (Figure 5; Head et al., 2003). We infer that thermogenic gas from the Oligocene is diluted with palaeo-microbial gas, retained in Late Oligocene to Miocene pore systems during burial beyond the base of the deep biosphere at 70-80 °C. The thermogenic methane fraction in the Pliocene gas accumulations investigated here is commonly around 50%, with the rest from a microbial origin. These data show that there is a pervasive flux of thermogenic gas from below the Messinian evaporites into and through the Nile Delta Pliocene.

Methane is the overwhelmingly prevalent alkane species throughout the Nile Delta's Pliocene section and gases generally contain < 2% C2+ at all stratigraphic levels above the Messinian. As commonly observed in mud volcanoes worldwide (Etiope et al., 2009), concentrations of C2+ tend to decrease towards shallower levels in our dataset, with the increased dryness accompanied by decreasing $\delta^{13}C1$. Phenomena related to differential alkane solubility such as 'water washing', although poorly understood (Schimmelmann et al., 2004) and thus not listed in Table 1, may lead to the formation of dry gases but associated isotope shifts are only in the order of < ± 1‰ (Boreham et al., 2001). Furthermore, we argue that limited fugacity gradients across phase boundaries in methane-saturated formation waters subdue the compositional impact in our case study. Instead, the dominance of methane with such light carbon isotope ratios is indicative of prevalent hydrogenotrophic methanogenesis (Table 1). This metabolic process follows the CO_2 reduction pathway, generating isotopically heavy carbon in residual CO_2 that is in some instances observed in conjunction with biodegradation indicators such as isotopically heavy C3+ (Figure 9). The increase in dryness towards shallower depths could therefore indicate a combination of (i) passive dilution of migrated thermogenic C2+ alkanes with primary microbial gas and (ii) concomitant methanogenic biodegradation of C2+ alkanes to secondary microbial gas (Table 1). On the other hand, the occurrence of carbon isotopically light CO_2 (B20; Figure 14) and C2 (B22; Figure 17) in strata where there has been no thermogenic charge and thus where these two processes are not relevant, suggests that here metabolic rates are low and microbial processes such as alkanogenesis are limited by the diagenetic decarboxylation of *in situ* organic matter. This establishes the broad trend of increasing $\delta^{13}C1$ with depth (Figure 5). The isotopic composition of ethane helps us to understand the nature of microbial carbon cycling in these sediments. The rather narrow range of $\delta^{13}C2$ values that we describe in our two case studies suggests two processes that exert counterbalancing carbon isotope effects on ethane. The most likely candidates, listed in Table 1, are biodegradation and acetoclastic alkanogenesis (Hinrichs et al., 2006), processes that occur together with methanogenic biodegradation (Jones et al., 2008). In our dataset, carbon isotope fingerprints dominated by acetoclastic alkanogenic activity such as ethanogenesis are rare but are seen, for example around

1300m in B22 (Figure 17). Since our data come from wells drilled with the objective of discovering commercial gas accumulations, we suggest that ethanogenesis may be common in the deep subsurface but is often unrecognised due to thermogenic charge that overprints pristine *in situ* microbial gas signatures, even at low concentrations of thermogenic ethane (Figure 7).

Our data also suggest that gases with heavy $\delta^{13}C\text{-}CO_2$ but regular thermogenic $\delta^{13}C3$ may also be subject to mutually obliterating carbon isotope effects. In this case, the carbon isotope shift that is commonly associated with C3 biodegradation (increasing $\delta^{13}C3$) is potentially buffered by concurrent propanogenesis (decreasing $\delta^{13}C3$). These counterbalancing isotope effects are only detectable in the data if thermogenic ethane and propane concentrations, respectively, are biodegraded to critically low concentrations that match the trace concentrations of their microbially generated equivalents (Figure 7). High ratios of $\delta^{13}C3$ (Figure 8), commonly acknowledged as residual indicators of biodegradation (James & Burns, 1984; Kinnaman et al., 2007), are only preserved if (i) metabolic turnover has outpaced C2+ supply from thermogenic charge and the microbial community enters a period of substrate shortage, and (ii) residual C2+ that carry the biodegradation signature accumulate in a free gas phase, away from connected water, that is inaccessible to further microbial cycling. These residual volumes of degraded C2+ may eventually fall below the detection limit of conventional gas sampling and laboratory analytical techniques, thereby obscuring the identification of microbial activity, particularly in sediments with high gas saturations (e.g. shallow reservoir in B22, Figure 17).

In summary, we observe that the mixing behaviour of trace ethane and propane concentrations in conjunction with their carbon isotope shifts supports widespread activity of methanogenic biodegradation in the Nile Delta subsurface. A geochemical footprint indicative of biodegradation of thermogenic C2+ is seen in cases where there is a limited charge rate of thermogenic gas, and where the building of a column of free gas phase reduces the rate of uptake, recycling and dilution by alkanogenic microbes; in contrast, classic methanogenic gas signatures (low concentrations of C2+, isotopically light C1 and C2) occur in bypassed strata where there is no thermogenic charge. These processes obscure traditional thermogenic gas maturity indicators (Berner & Faber, 1996; Clayton, 1991) and introduce the risk of mistaking (i) biodegradation footprints with higher maturity gases and (ii) alkanogenic footprints with lower maturity gases.

We cannot quantify the fraction of secondary microbial gas generated by methanogenic biodegradation because the associated $\delta^{13}C1$ fingerprint is intermediate to the end-member carbon isotope ratios of primary methane (Milkov, 2011; Milkov & Etiope, 2018). Instead, we stress that $\delta^{13}C1$ of secondary microbial origin depends on (i) the initial $\delta^{13}C1$ of already admixed primary gases prior to onset of biodegradation and (ii) on the degree of biodegradation which can induce an isotope shift of up to -15‰ in a closed-system environment (Jones et al., 2008). Considering the total spread of 35‰ between the thermogenic and primary microbial methane carbon isotope end-members, excessive methanogenic biodegradation of a 1:1 primary gas mixture would be capable of shifting the bulk $\delta^{13}C1$ value close to the primary microbial end-member. In other words, the relative proportion of secondary microbial methane may be much larger than expected from the isotope dataset at hand. From a material balance point of view, however, considering that C1 is usually around 70% by weight of the initial thermal alkane composition, even if all the C2+ was converted to secondary microbial methane it is still only going to be some 30% of the total thermogenic gas, and thus maximum 15% of the methane encountered in the mixed gas reservoirs that we discussed in our case studies.

5.2 Migration mechanisms and pathways

The gas geochemical data within this study are remarkable in their quality, quantity and vertical resolution. Although they have the inevitable restriction that they are profiles from single wells, the

high sampling density and the fact that samples were taken in both mud-rich and sand-rich units, allows some unique insights into likely migration and leakage pathways through lithologically heterogeneous, dipping, sedimentary systems.

Gas migration may occur via (a) lateral migration along coarser-grained units with relatively low capillary entry pressures, (b) vertical migration at structural highs and (c) sub-vertical migration along fault systems, potentially bypassing the stratigraphy (Cartwright et al., 2007). Although we cannot unequivocally define lateral migration from purely vertical profiles, we infer from the carbon isotope data that much of the charge to structural highs is via lateral migration along dipping, coarser-grained, lower capillary entry pressure sedimentary units (Figure 15, Figure 19). The key evidence for this is (a) the lack of thermogenic gas at the very base of the wells, ruling out strictly vertical migration of thermogenic gas from the deeper subsurface; (b) the occurrence of compositionally distinct gases in individual sand-rich units, showing that the sedimentary pore system is not flushed and compositionally equilibrated (e.g. B24, Figure 18); (c) the occurrence of pure microbial gas in some of the mud-rich units which stratigraphically separate coarser-grained units that contain thermogenic gas (e.g. B22 and B24; Figure 17 and Figure 18).

The occurrence of thermogenic gas in many of the mud-rich units indicates that vertical migration/leakage is occurring through these units at structural highs. However, the nature of the isotope profiles through the mud-rich units differ, which we suggest reflects the nature and pervasiveness of the vertical migration process. In B19 (Figure 13), and between 1580 and 1730 metres depth in B22 (Figure 17), the isotopic composition of the gas in the mud-rich sections is similar throughout, indicating gas with a constant composition. We suggest that this profile indicates pervasive vertical migration through the approximately one hundred metre sections of mud-rich sediments.

A second type of isotope profile is represented by steadily decreasing percentages of thermogenic gas over distances of 60-200 metres through mud-rich sequences overlying sand-rich intervals (B22 and B24; Figure 17 and Figure 18). We interpret these trends as indicating minor vertical migration/leakage, in which the mixed thermogenic-microbial gas within the sandstone units is leaking into mud-rich units which contain pre-existing microbial gas.

In a third profile type, increasing percentages of thermogenic gas are observed from the centre of mud-rich sequences up to gas accumulations in sand-rich units (B22 and B24; Figure 17 and Figure 18). One explanation for this trend is that the increasing proportion of thermogenic gas reflects a series of lateral, individual contributions of thermogenic-rich gas along thin beds of coarser-grained sediment, with an increasingly thermogenic gas leaking vertically from thin bed to thin bed. Others have suggested that this type of curved profile may reflect composite diffusion-advection equilibria (Leith et al., 1993), possibly governed by microbial carbon cycling (Whiticar, 1999). However, we caution that these trends may simply reflect the occurrence of recycled gases in re-injected drilling muds, since this is most likely to be seen when drilling past a highly gas-saturated reservoir section into underlying mudstones with low gas contents.

Measured capillary entry pressures of centimetre-scale, homogeneous muds in this area (Böker, 2011), and in similar muds elsewhere (Dewhurst et al., 1998; Aplin & Moore, 2016), suggest that they are capable of retaining gas columns > 500m. Since gas columns of these magnitudes do not occur in this area, how can we explain the occurrence of migrated gas within the mud-rich sections? We cannot definitively answer this question, but one possibility is that small-scale lithological heterogeneities within the sediment system, and the occurrence of small-scale sand injectites (e.g. Figure 12), create connected, lower capillary entry pressure pathways along which gas will preferentially percolate (Carruthers and Ringrose, 1998). Where heterogeneities, injectites and the occurrence of relatively coarser-grained, lower capillary pressure sediments are more common (B19

and B20), vertical leakage will be both more pervasive and faster than where they are rarer (B22 and B24).

We also speculate that capillary entry pressures may not be a critical control on migration, and that the flow of gas through the mud-rich sequences could be primed by the presence of filaments and pockets of residual, free microbial gas. In this case, capillary entry pressures related to the occurrence of water-filled pores lose their importance (Sheng et al., 1999) and the flux of gas through the muds is more closely linked to permeability structures. The occurrence of free gas within the most permeable pore systems of heterogeneous mudstones is a realistic assumption given the widespread accumulation of gases in nearby sandstone reservoirs, and the fact that microbial gas is both generated within and expelled from the mud-rich sections. This implies that pore waters within the mud-rich sections must be gas-saturated and that some free gas will be trapped within the muds. Here, microbes populate pore systems with the most favourable interconnectivity (Fredrickson et al., 1997; Krumholz et al., 1997; Rebata-Landa & Santamarina, 2006) and microbial abundance has been shown to scale with permeability (Tanikawa et al., 2018). These observations suggest that preferred migration routes inside mudstones are populated with microbes capable of generating free gases (Clayton, 1992; Clayton, 2010) that would most effectively drain by flow through filaments of connected gas phase (Schowalter, 1979), possibly during episodic percolation events (Carruthers & Ringrose, 1998). Such distributed fractal flow systems would not be detectable on seismic, which more readily images focused bypass features such as large-scale sandstone injectites and gas chimneys (Cartwright et al., 2007; Cartwright, 2010). Preferential pathways, plus the fact that gas will exploit only the larger pores in any sediment, would explain our observation that microbial gas continues to be present in the mud-rich units, indicating that the pore system is not fully flushed by migrating gas. This hypothesis is supported by the inferred retention of microbial gas at depths below the present-day limits of the deep biosphere, as discussed earlier in Section 5.1.

Bypass features within the study area are mud volcanoes (Figure 2) and faults. Well B22 is located some 2000m away from the centre of the North Alex mud volcano (Figure 16) which carries relatively pristine thermogenic gas (Figure 6, Figure 7a and Figure 8) and may be the deeper conduit for the migration of thermogenic gas to this area (Prinzhofer & Deville, 2013). The large δ^{13}C1 range in gases sampled inside and above these chimney features (e.g. Figure 5) imply that near-surface processes such as C1-biodegradation coupled to sulphate reduction, often associated with extreme δ^{13}C depletion (Yoshinaga et al., 2014; Knittel & Boetius, 2009) (see Figure 4c), alter the isotopic signature of gases arriving from depth. These observations, together with the temporal variation in the chemical signatures of seafloor seepage (Mastalerz et al., 2007), support an episodic or pulse-like activity of Nile Delta mud volcanoes with dormant and active phases. This view is consistent with the concept that basin loading is largely controlled by episodic slope failures that trigger turbidites and related mass flow phenomena (Loncke et al., 2008). These slope failures can lead to rapid pressure and stress changes which may result in the formation of pockmarks at the seabed (Gay et al., 2003; Judd & Hovland, 2007) and sub-seismic bypass features such as the sandstone intrusions shown in Figure 12.

On the other hand, considering that our gas profiles intercept a number of seismic-scale faults within mud-rich sequences, geochemical data from this study offer little support for along-fault migration despite recurring suggestions that faults can act as sub-vertical conduits for gas in this area (Kamel et al., 1998; Loncke et al., 2004; Garziglia et al., 2008; Dupré et al., 2010; Khaled et al., 2014; Ligtenberg, 2005). One exception may be the slight perturbation toward wetter thermogenic gases at the fault-intercept in the topseal of B22 (Figure 17), which could be interpreted as the delivery of a compositionally distinct gas along the fault. All other faults appear to act as flow barriers, for example by preventing the influx of thermogenic gas into the methanogenic and alkanogenic mudstone habitat (inter-reservoir in B22), or by restricting pressure communication between the channel legs, as in the Horus case study.

Although our dataset cannot quantify flux we note that the differences in geochemical signatures which occur over a few metres indicate a lack of compositional equilibration which, in a system which is not being actively charged with new gas, would be expected to occur, even by diffusion, on timescales of less than a million years (England, 1990). Furthermore, in structural configurations where the rates of charge and microbial alteration of gas are occurring on comparable timescales, both processes can be observed in the geochemical signatures. The Pliocene of the Nile Delta is thus clearly a system into which gas is being charged, accumulated, biodegraded and leaked on geologically short periods of time.

6 Conclusions

We draw the following conclusions:

1. Thermogenic gas in the west Nile region derives from a sub-Messinian source and mixes with primary microbial, hydrogenotrophic, methane-rich gas in the Plio-Pleistocene section.
2. Alkane carbon isotopes provide a reliable proxy for mixing ratios of thermogenic and microbial gases only if the end-member gases have similar molecular compositions.
3. Microbially mediated isotope shifts in individual alkanes obscure the maturity signal from the source rock. However, careful analysis of a regional bulk gas dataset allows maturity to be assessed if the predominant end-member chemical compositions can be identified. We have identified an Oligocene source signature that is diluted down to 80% thermogenic gas by palaeo-microbial gases below the regional Messinian seal. Pliocene reservoirs contain no more than 50% migrated thermogenic gas.
4. Pristine thermogenic gases are rare and wet gas components of the Pliocene gas mixtures tend to disappear at shallower stratigraphic levels, suggesting that a large fraction of the wet gas components from sub-Messinian thermogenic sources are metabolized via methanogenic biodegradation. A fraction of microbial methane within commercial gas accumulations therefore has a secondary microbial origin. Material balance suggests that this fraction does not exceed 15% of the reservoir gases in our case studies.
5. The effect of biodegradation on ethane and propane carbon isotope ratios may be buffered by syntrophic alkanogenesis, indicating closed-system alkane cycling. Classic biodegradation indicators (heavy δ^{13}C3+) are preserved only if the products of biodegradation are removed from sites of alkanogenesis, e.g. inside gas columns, and at times when thermogenic charge and organic acid formation are outpaced by microbial turnover. Ethane tends to follow the C3 isotope shifts but to a much lesser extent, probably due to *in situ* microbial ethane being produced at higher rates than microbial propane. As ethane is the second most common alkane in the system, the δ^{13}C2 footprint is buffered by its dominantly thermogenic origin from a narrow source rock maturity window and therefore remains isotopically unchanged unless metabolic rates of ethane destruction outpace thermogenic ethane supply. We stress that the process of ethane biodegradation is currently understood for aerobic conditions only (Kinnaman et al., 2007).
6. *In situ* generation of microbial gas in the pore-space of heterogeneous mudstone units facilitates percolation of migrating gases that replenish C2+ components and sustains biodegradation pathways in syntrophic microbial communities. Pooling of microbial gas reduces the distance that migrating gases need to overcome by percolation through a water-saturated medium.
7. There is limited geochemical evidence for migration along or across faults which cross-cut mud-rich sequences. Lateral migration along sands/silts delivers gas to structural highs, where leakage occurs vertically along focussed pathways through heterogeneous mud-rich sediments.

8. High resolution changes in gas composition along vertical profiles at structural highs suggest an unequilibrated gas system which is being actively charged. In some structures, rates of charge and of microbial alteration of gas are broadly similar; in others, rates of charge exceed rates of microbial alteration.

Acknowledgements

A significant part of this work was funded by the Caprocks JIP with sponsorship from Anadarko, BG, BHP Billiton, BP, Chevron, Conoco Phillips, Eni, Petrobras, Shell, Statoil, Total and the BERR. Special appreciation is expressed to BP for supplying samples and data, and to its management for permission of publication. We would also like to thank Alexei Milkov and four anonymous reviewers that helped to improve this manuscript.

References

Abdel Aal, A. et al., 2000. Tectonic evolution of the Eastern Mediterranean Basin and its significance for hydrocarbon prospectivity in the ultradeepwater of the Nile Delta. *The Leading Edge,* 19(10), pp. 1086-1102.

Abd-Elfattah, N. & Fahmy, R. M., 2017. Reducing the risk of hydrocarbon exploration and lithology characterization — using a neural network approach in the West Delta Deep Marine Concession Area, Offshore Nile Delta, Egypt. *First Break,* 35(7), pp. 41-49.

Aitken, C. M., Jones, D. M. & Larter, S. R., 2004. Anaerobic hydrocarbon biodegradation in deep subsurface oil reservoirs. *Nature,* 431(7006), pp. 291-294.

Al-Balushi, A. N., Neumaier, M., Fraser, A. J. & Jackson, C. A.-L., 2016. The impact of the Messinian salinity crisis on the petroleum system of the Eastern Mediterranean: a critical assessment using 2D petroleum system modelling. *Petroleum Geoscience,* 22(4), pp. 357-379.

Andresen, B., Throndsen, T., Råheim, A. & Bolstad, J., 1995. A comparison of pyrolysis products with models for natural gas generation. *Chemical Geology,* 126(3-4), pp. 261-280.

Aplin, A. C. & Larter, S. R., 2005. Fluid Flow, Pore Pressure, Wettability, and Leakage in Mudstone Cap Rocks. In: P. Boult & J. Kaldi, red. *Evaluating fault and cap rock seals.* Tulsa: AAPG, Hedberg Series 2, pp. 1-12.

Aplin, A. C. & Moore, J. K., 2016. Observations of pore systems of natural siliciclastic mudstones. *The Clay Minerals Society Workshop Lectures Series,* Volume 21, pp. 31-42.

Berner, U. & Faber, E., 1996. Empirical carbon isotope/maturity relationships for gases from algal kerogens and terrigeneous organic matter, based on dry, open-system pyrolysis. *Organic Geochemistry,* 24(10-11), pp. 947-955.

Bertoni, C., Cartwright, J. & Hermanrud, C., 2013. Evidence for large-scale methane venting due to rapid drawdown of sea level during the Messinian Salinity Crisis. *Geology,* 41(3), pp. 371-374.

Böker, U., 2011. *Controls on natural gas migration in the Western Nile Delta fan.* PhD thesis red. Newcastle Upon Tyne: Newcastle University.

Boreham, C. J., Golding, S. D. & Glikson, M., 1998. Factors controlling the origin of gas in Australian Bowen Basin coals. *Organic Geochemistry,* 29(1-3), pp. 347-362.

Boreham, C. J., Hope, J. M. & Hartung-Kagi, B., 2001. Understanding source distribution and preservation of Australian natural gas: a geochemical perspective. *APPEA Journal,* 41(1200), pp. 523-547.

Carruthers, D. J. & Ringrose, P. S., 1998. Secondary oil migration: oil-rock contact volumes, flow behaviour and rates. In: J. Parnell, red. *Dating and Duration of Fluid Flow and Fluid-Rock Interaction.* London: Geological Society of London, Special Publications 144, pp. 205-220.

Cartwright, J., 2010. Regionally extensive emplacement of sandstone intrusions: a brief review. *Basin Research,* 22(4), pp. 502-516.

Cartwright, J., Huuse, M. & Aplin, A., 2007. Seal bypass systems. *AAPG Bulletin,* 91(8), pp. 1141-1166.

Cerling, T. E., Kip Solomon, D., Quade, J. & Bowman, J. R., 1991. On the isotopic composition of carbon in soil carbon dioxide. *Geochimica et Cosmochimica Acta,* 55(11), pp. 3403-3405.

Chamley, H., 1989. *Clay Sedimentology.* 1st red. Berlin Heidelberg New York: Springer.

Chung, H. M., Gormly, J. R. & Squires, R. M., 1988. Origin of gaseous hydrocarbons in subsurface environments: theoretical considerations of carbon isotope distribution. *Chemical Geology,* 71(1-3), pp. 97-103.

Chung, H. M. & Sackett, W. M., 1980. Carbon isotope effects during the pyrolytic formation of early methane from carbonaceous materials. *Physics and Chemistry of the Earth,* Volume 12, pp. 705-710.

Clayton, C., 1991. Carbon isotope fractionation during natural gas generation from kerogen. *Marine and Petroleum Geology,* 8(2), pp. 232-240.

Clayton, C., 1992. Source Volumetrics of Biogenic Gas Generation. In: R. Vially, red. *Bacterial Gas.* Paris: Editions Technip, pp. 191-204.

Clayton, C., 2010. *Incorporation of biogenic gas generation into petroleum system models.* London, Geological Society of London.

Coleman, D. D., Risatti, J. B. & Schoell, M., 1981. Fractionation of carbon and hydrogen isotopes by methane-oxidizing bacteria. *Geochimica et Cosmochimica Acta,* 45(7), pp. 1033-1037.

Davis, J. B. & Squires, R. M., 1954. Detection of microbially produced gaseous hydrocarbons other than methane. *Science,* 119(3019), pp. 381-382.

de Graaf, W., Wellsbury, P., Parkes, R. J. & Cappenberg, T. E., 1996. Comparison of acetate turnover in methanogenic and sulfate-reducing sediments by radiolabeling and stable isotope labeling and by use of specific inhibitors: Evidence for isotopic exchange. *Applied and Environmental Microbiology,* 62(3), pp. 772-777.

Dewhurst, D. N., Aplin, A. C., Sarda, J. P. & Yang, Y., 1998. Compaction-driven evolution of poroperm in natural mudstones: an experimental study. *Journal of Geophysical Research,* 103(B1), pp. 651-661.

Dolson, J. C. et al., 2001. Chapter 23: The petroleum potential of Egypt. In: J. T. J. M. W. Downey, red. *Petroleum Provinces of the Twenty-first Century - AAPG Memoir Series, Vol. 74.* Tulsa: AAPG, pp. 453-482.

Dupré, S. et al., 2010. Widespread active seepage activity on the Nile Deep Sea Fan (offshore Egypt) revealed by high-definition geophysical imagery. *Marine Geology,* 275(1-4), pp. 1-19.

El Diasty, W. S. & Moldowan, J. M., 2013. The Western Desert versus Nile Delta: A comparative molecular biomarker study. *Marine and Petroleum Geology,* Volume 46, pp. 319-334.

El Nady, M. M., 2007. Organic Geochemistry of Source Rocks, Condensates, and Thermal Geochemical Modeling of Miocene Sequence of Some Wells, Onshore Nile Delta, Egypt. *Petroleum Science and Technology,* 25(6), pp. 791-818.

El-Ella, R. A., 1990. The Neogene-Quarternary Section in the Nile Delta, Egypt: Geology and Hydrocarbon Potential. *Petroleum Geology,* 13(3), pp. 329-340.

England, W. A., 1990. The organic geochemistry of petroleum reservoirs. *Organic Geochemistry,* 16(1-3), pp. 415-425.

Eruteya, O. E. et al., 2015. Intra- to post-Messinian deep-water gas piping in the Levant Basin, SE Mediterranean. *Marine and Petroleum Geology,* Volume 66 (Part 1), pp. 246-261.

Etiope, G. et al., 2009. Evidence of subsurface anaerobic biodegradation of hydrocarbons and potential secondary methanogenesis in terrestrial mud volcanoes. *Marine and Petroleum Geology,* 26(9), pp. 1692-1703.

Feinstein, S. et al., 2002. Genetic characterization of gas shows in the east Mediterranean offshore of southwest Israel. *Organic Geochemistry,* 33(12), pp. 1401-1413.

Feisthauer, S. et al., 2010. Isotopic fingerprinting of methane and CO2 formation from aliphatic and and aromatic hydrocarbons. *Organic Geochemistry,* 41(5), pp. 482-490.

Fredrickson, J. K. et al., 1997. Pore-size constraints on the activity and survival of subsurface bacteria in a late cretaceous shale-sandstone sequence, northwestern New Mexico. *Geomicrobiology Journal,* 14(3), pp. 183-202.

Friedrich, H. U. & Jüntgen, H., 1972. Some measurements of the 13C/12C ratio in methane or ethane desorbed from hard coal or released by pyrolysis. In: H. W. H. von Gaertner, red. *Advances in Organic Geochemistry (1971).* Oxford: Pergamon, pp. 639-646.

Fuex, A. N., 1977. The use of stable carbon isotopes in hydrocarbon exploration. *Geochemical Exploration,* Volume 7, pp. 155-188.

Fuex, A. N., 1980. Experimental evidence against an appreciable isotopic fractionation of methane during migration. *Physics and Chemistry of the Earth (Part C),* Volume 12, pp. 725-732.

Galimov, E. M., 1975. *Carbon isotopes in oil-gas geology (NASA TT F–682).* Washington D.C.: NASA.

Garfunkel, Z., 1998. Constrains on the origin and history of the Eastern Mediterranean basin. *Tectonophysics,* 298(1-3), pp. 5-35.

Garziglia, S. et al., 2008. Mass-transport deposits on the Rosetta province (NW Nile deep-sea turbidite system, Egyptian margin): Characteristics, distribution, and potential causal processes. *Marine Geology,* 250(3-4), pp. 180-198.

Gay, A. et al., 2003. Sonuous pockmark belt as indicator of a shallow buried turbiditic channel on the lower slope of the Congo basin, West African margin. *Geological Society of London Special Publications,* Volume 216, pp. 173-189.

Grant, N. J. & Whiticar, M. J., 2002. Stable carbon isotopic evidence for methane oxidation in plumes above Hydrate Ridge, Cascadia Oregon Margin. *Global Biogeochemical Cycles,* 16(4), pp. 71-1–71-13.

Grassia, G. S. et al., 1996. A systematic survey for thermophilic fermentative bacteria and archaea in high temperature petroleum reservoirs. *FEMS Microbiology Ecology,* 21(1), pp. 47-58.

Hanafy, S., Nimmagadda, S. L., Mahmoud, S. E. & Mabrouk, W. M., 2017. New insights on structure and stratigraphic interpretation for assessing the hydrocarbon potentiality of the offshore Nile Delta basin, Egypt. *Journal of Petroleum Exploration and Production Technology,* 7(2), pp. 317-339.

Haq, B. U., Hardenbol, J. & Vail, P. R., 1988. Mesozoic and Cenozoic Chronostratigraphy and Cycles of Sea-Level Change. In: K. C. Wilgus, et al. red. *Sea-Level Changes: An Integrated Approach.* SEPM Special Publication red. Tulsa(Oklahoma): SEPM, pp. 71-108.

Hardenbol, J. et al., 1998. Mesozoic and Cenozoic Sequence Chronostratigraphic Framework of European Basins. In: P. de Graciansky, J. Hardenbol, T. Jacquin & P. R. Vail, red. *Mesozoic and Cenozoic Sequence Stratigraphy of European Basins.* Tulsa: SEPM Special Publication 60, pp. 3-13.

Head, I. M., Jones, D. M. & Larter, S. R., 2003. Biological activity in the deep subsurface and the origin of heavy oil. *Nature,* 426(6964), pp. 344-352.

He, K., Zhang, S., Mi, J. & Zhang, W., 2018. The evolution of chemical groups and isotopic fractionation at different maturation stages during lignite pyrolysis. *Fuel,* Volume 211, pp. 492-506.

Hinrichs, K.-U.et al., 2006. Biological formation of ethane and propane in the deep marine subsurface. *Proceedings of the National Academy of Sciences of the United States of America,* 103(40), pp. 14684-14689.

James, A. T., 1983. Correlation of natural gas by use of carbon isotopic distribution between hydrocarbon components. *AAPG Bulletin,* 67(7), pp. 1176-1191.

James, A. T. & Burns, B. J., 1984. Microbial Alteration of Subsurface Natural Gas Accumulations. *AAPG Bulletin,* 68(8), pp. 957-960.

Jones, D. M. et al., 2008. Crude-oil biodegradation via methanogenesis in subsurface petroleum reservoirs. *Nature,* 451(7175), pp. 176-180.

Jørgensen, B. B. & D'Hondt, S., 2006. A Starving Majority Deep Beneath the Seafloor. *Science,* 314(5801), pp. 932-934.

Judd, A. & Hovland, M., 2007. *Seabed Fluid Flow.* 2009 red. Cambridge: Cambridge University Press.

Kamel, H., Eita, T. & Sarhan, M., 1998. *Nile Delta hydrocarbon potentiality.* Cairo, EGPC, pp. 485-503.

Katz, B. J., 2011. Microbial processes and natural gas accumulations. *The Open Geology Journal,* Volume 5, pp. 75-83.

Keshta, S., Metwalli, F. I. & Al Arabi, H. S., 2012. Analysis of Petroleum System for Exploration and Risk Reduction in Abu Madi/El Qar'a Gas Field, Nile Delta, Egypt. *International Journal of Geophysics,* 2012(Article ID 187938), pp. 1-10.

Khaled, K. A., Attia, G. M., Metwalli, F. I. & Fagelnour, M. S., 2014. Subsurface Geology and Petroleum System in the Eastern Offshore Area, Nile Delta, Egypt. *Journal of Applied Sciences Research,* 10(4), pp. 254-270.

Kieft, T. L. et al., 1993. Microbial abundance and activities in relation to water potential in the vadose zones of arid and semiarid sites. *Microbial Ecology,* 26(1), pp. 59-78.

Kinnaman, F. S., Valentine, D. L. & Tyler, S. C., 2007. Carbon and hydrogen isotope fractionation associated with the aerobic microbial oxidation of methane, ethane, propane and butane. *Geochimica et Cosmochimica Acta,* 71(2), pp. 271-283.

Kniemeyer, O. et al., 2007. Anaerobic oxidation of short-chain hydrocarbons by marine sulphate-reducing bacteria. *Nature,* 449(7164), pp. 898-901.

Knittel, K. & Boetius, A., 2009. Anaerobic Oxidation of Methane: Progress with an Unknown Process. *Annual Review of Microbiology,* Volume 63, pp. 311-334.

Krooss, B. M., 1986. Diffusion of C1 to C5 hydrocarbons in water-saturated sedimentary rocks. *Erdöl und Kohle – Erdgas – Petrochemie,* 39(9), pp. 399-402.

Krumholz, L. R., McKinley, J. P., Ulrich, G. A. & Suflita, J. M., 1997. Confined subsurface microbial communities in Cretaceous rock. *Nature,* 386(6620), pp. 64-66.

Larson, T. E. & Breecker, D. O., 2014. Adsorption isotope effects for carbon dioxide from illite- and quartz-packed column experiments. *Chemical Geology,* Volume 370, pp. 58-68.

Leith, T. L. et al., 1993. Recognition of caprock leakage in the Snorre Field, Norwegian North Sea. *Marine and Petroleum Geology,* 10(1), pp. 29-41.

Lide, D. R., 2005. *Diffusion of Gases in Water. In CRC Handbook of Chemistry and Physics, David R. Lide (ed.), Internet Version 2005, <http://www.hbcpnetbase.com>,* Boca Raton, FL: CRC Press.

Ligtenberg, J. H., 2005. Detection of fluid migration pathways in seismic data: implications for fault seal analysis. *Basin Research,* 17(1), pp. 141-153.

Loncke, L. et al., 2008. Multi-scale slope instabilities along the Nile deep-sea fan, Egyptian margin: A general overview. *Marine and Petroleum Geology,* 26(5), pp. 633-646.

Loncke, L. et al., 2006. The Nile deep-sea fan: An example of interacting sedimentation, salt tectonics, and inherited subsalt paleotopographic features. *Marine and Petroleum Geology,* 23(3), pp. 297-315.

Loncke, L., Mascle, J. & Fanil Scientific Parties, 2004. Mud volcanoes, gas chimneys, pockmarks and mounds in the Nile deep-sea fan (Eastern Mediterranean): geophysical evidences. *Marine and Petroleum Geology,* 21(6), pp. 669-689.

Lückge, A., Kastner, M., Littke, R. & Cramer, B., 2002. Hydrocarbon gas in the Costa Rica subduction zone: Primary composition and post-genetic alteration. *Organic Geochemistry,* 33(8), pp. 933-943.

Mastalerz, V., de Lange, G., Dählmann, A. & Feseker, T., 2007. Venting at Isis mud volcano, offshore Egypt: origin and migration of hydrocarbons. *Chemical Geology,* 246(1-2), pp. 87-106.

Mastalerz, V., de Lange, G. J. & Dählmann, A., 2009. Differential aerobic and anaerobic oxidation of hydrocarbon gases discharged at mud volcanoes in the Nile deep-sea fan. *Geochimica et Cosmochimica Acta,* 73(13), pp. 3849-3863.

Mattavelli, L., Ricchiuto, T., Grignani, D. & Schoell, M., 1983. Geochemistry and Habitat of Natural Gases in Po Basin, Northern Italy. *AAPG Bulletin,* 67(12), pp. 2239-2254.

Milkov, A. V., 2011. Worldwide distribution and significance of secondary microbial methane formed during petroleum biodegradation in conventional reservoirs. *Organic Geochemistry,* 42(2), pp. 184-207.

Milkov, A. V. & Etiope, G., 2018. Revised genetic diagrams for natural gases based on a global dataset of >20,000 samples. *Organic Geochemistry,* Volume 125, pp. 109-120.

Nelson, J. S. & Simmons, E. C., 1992. The quantification of diffusive hydrocarbon losses through cap rocks of natural gas reservoirs - a reevaluation: discussion. *AAPG Bulletin,* 76(11), pp. 1839-1841.

Oremland, R. S., Whiticar, M. J., Strohmaier, F. E. & Kiene, R. P., 1988. Bacterial ethane formation from reduced ethylated compounds in anoxic sediments. *Geochimica et Cosmochimica Acta,* 52(7), pp. 1895-1904.

Pallasser, R. J., 2000. Recognizing biodegradation in gas/oil accumulations through the δ13C compositions of gas components. *Organic Geochemistry,* 31(12), pp. 1363-1373.

Pernaton, E., Prinzhofer, A. & Schneider, F., 1996. Reconsideration of methane signature as a criterion for the genesis of natural gas: influence of migration on isotopic signature. *Revue de l'Institut Français du Pétrole,* 51(5), pp. 635-651.

Prinzhofer, A. & Deville, E., 2013. Origins of hydrocarbon gas seeping out from offshore mud volcanoes in the Nile delta. *Tectonophysics,* Volume 591, pp. 52-61.

Prinzhofer, A. & Huc, A. Y., 1995. Genetic and post-genetic molecular and isotopic fractionations in natural gases. *Chemical Geology,* 126(3-4), pp. 281-290.

Prinzhofer, A., Mello, M. R. & Takaki, T., 2000. Geochemical Characterization of Natural Gas: A Physical Multivariable Approach and its Applications in Maturity and Migration Estimates. *AAPG Bulletin,* 84(8), pp. 1152-1172.

Prinzhofer, A. & Pernaton, E., 1997. Isotopically light methane in natural gases: bacterial imprint or segregative migration?. *Chemical Geology,* 142(3-4), pp. 193-200.

Quigley, T. M., Mackenzie, A. S. & Gray, J. R., 1987. Kinetic theory of petroleum generation. In: B. Doligez, ed. *Migration of Hydrocarbons in Sedimentary Basins: 3rd IFP Exploration and Production Research Conference, Carcans.* Paris: Éditions Technip, pp. 649-665.

Rebata-Landa, V. & Santamarina, J. C., 2006. Mechanical limits to microbial activity in deep sediments. *Geochemistry Geophysics Geosystems,* 7(11), pp. 1-12.

Rice, D. D. & Claypool, G. E., 1981. Generation, accumulation and resource potential of biogenic gas. *AAPG Bulletin,* 65(1), pp. 5-25.

Risk, D. & Kellman, L., 2008. Isotopic fractionation in non-equilibrium diffusive environmnets. *Geophysical Research Letters,* 35(2), pp. L02403 (1-4).

Röling, W. F., Head, I. M. & Larter, S. R., 2003. The microbiology of hydrocarbon degradation in subsurface petroleum reservoirs: perspectives and prospects. *Research in Microbiology,* 154(5), pp. 321-328.

Schimmelmann, A., Lewan, M. D. & Wintsch, R. P., 1999. D/H isotope ratios of kerogen, bitumen, oil, and water in hydrous pyrolysis of source rocks containing kerogen types I, II, IIS, and III. *Geochimica et Cosmochimica Acta,* 63(22), pp. 3751-3766.

Schimmelmann, A. et al., 2004. D/H ratios in terrestrially sourced petroleum systems. *Organic Geochemistry,* 35(10), pp. 1169-1195.

Schloemer, S., Elbracht, J., Blumenberg, M. & Illing, C. J., 2016. Distribution and origin of dissolved methane, ethane and propane in shallow groundwater of Lower Saxony, Germany. *Applied Geochemistry,* Volume 67, pp. 118-132.

Schloemer, S. & Krooss, B. M., 2004. Molecular transport of methane, ethane and nitrogen and the influence of diffusion on the chemical and isotopic composition of natural gas accumulations. *Geofluids,* 4(1), pp. 81-108.

Schoell, M., 1983. Genetic characterization of natural gases. *AAPG Bulletin,* 67(12), pp. 2225-2238.

Schoell, M., Jenden, P. D., Beunas, M. A. & Coleman, D. D., 1993. Isotope analysis in gas field and gas storage operations (SPE-26171-MS). *SPE Gas Technology Symposium*, 28-30 June, p. 10.

Schowalter, T. T., 1979. Mechanics of Secondary Hydrocarbon Migration and Entrapment. *AAPG Bulletin,* 63(5), pp. 723-760.

Shaaban, F. et al., 2006. Source-rock Evaluation and Basin Modelling in NE Egypt (NE Nile Delta and Northern Sinai). *Petroleum Geology,* 29(2), pp. 103-124.

Sharaf, L. M., 2003. Source Rock Evaluation and Geochemistry of Condensates and Natural Gases, offshore Nile Delta, Egypt. *Petroleum Geology,* 26(2), pp. 189-209.

Sheng, J. J., Maini, B. B., Hayes, R. E. & Tortike, W. S., 1999. Critical review of foamy oil flow in porous media. *Transport in Porous Media,* 35(2), pp. 157-187.

Stahl, W. J., 1977. Carbon and nitrogen isotopes in hydrocarbon research and exploration. *Chemical Geology,* 20(2), pp. 121-149.

Takahashi, K. U. & Suzuki, N., 2017. Semi-open and closed system pyrolysis of Paleogene coal for evaluating the timing of hydrocarbon gas expulsion. *International Journal of Coal Geology,* Volume 178, pp. 100-109.

Takahashi, K. U., Suzuki, N. & Saito, H., 2014. Compositional and isotopic changes in expelled and residual gases during anhydrous closed-system pyrolysis of hydrogen-rich Eocene subbituminous coal. *International Journal of Coal Geology,* Volume 127, pp. 14-23.

Tanikawa, W. et al., 2018. Geophysical constraints on microbial biomass in subseafloor sediments and coal seams down to 2.5 km off Shimokita Peninsula, Japan. *Progress in Earth and Planetary Science,* 5(58), pp. 1-17.

Taylor, S. W., Sherwood Lollar, B. & Wassenaar, L. I., 2000. Bacteriogenic Ethane in Near-Surface Aquifers: Implications for Leaking Hydrocarbon Well Bores. *Environmental Science and Technology,* 34(22), pp. 4727-4732.

Tyler, S. C., Crill, P. M. & Brailsford, G. W., 1994. 13C/12C Fractionation of methane during oxidation in a temperate forested soil. *Geochimica et Cosmochimica Acta,* 58(6), pp. 1625-1633.

Vandré, C., Cramer, B., Gerling, P. & Winsemann, J., 2007. Natural gas formation in the western Nile delta (Eastern Mediterranean): Thermogenic versus microbial. *Organic Geochemistry,* 38(4), pp. 523-539.

Vieth, A., Mangelsdorf, K., Sykes, R. & Horsfield, B., 2008. Water extraction of coals - potential for estimating low molecular weight organic acids as carbon feedstock for the deep terrestrial biosphere. *Organic Geochemistry,* 39(8), pp. 985-991.

Villinski, J., 2013. *Unusual but Effective Petroleum Systems - Disseminated Terrestrial Organic Matter of the Upper Oligocene as the Primary Source Rock, Offshore Nile Delta, Egypt. AAPG Search and Discovery Article #90161©2013.* Barcelona, AAPG.

Vinson, D. S. et al., 2017. Microbial methane from in situ biodegradation of coal and shale: A review and reevaluation of hydrogen and carbon isotope signatures. *Chemical Geology,* Volume 453, pp. 128-145.

Weissman, S. & DuBro, G. A., 1971. Diffusion Coefficients for CO2–CH4. *The Journal of Chemical Physics,* 54(5), pp. 1881-1883.

Wellsbury, P. et al., 1997. Deep marine biosphere fuelled by increasing organic matter availability during burial and heating. *Nature,* 388(6642), pp. 573-576.

Whiticar, M. J., 1999. Carbon and hydrogen isotope systematics of bacterial formation and oxidation of methane. *Chemical Geology,* 161(1-3), pp. 291-314.

Yoshinaga, M. Y. et al., 2014. Carbon isotope equilibration during sulphate-limited anaerobic oxidation of methane. *Nature Geoscience,* 7(3), pp. 190-194.

Yoshioka, H. et al., 2015. Methane production potential of subsurface microbes in Pleistocene sediments from a natural gas field of the dissolved-in-water type, central Japan. *Chemical Geology,* Volume 419, pp. 92-101.

Younes, M. A.-A., 2015. Natural Gas Geochemistry in the Offshore Nile Delta, Egypt. In: V. Patel, red. *Advances in Petrochemicals.* Rijeka: InTech, pp. 27-40.

Zeikus, J. G. & Winfrey, M. R., 1976. Temperature limitation of methanogenesis in aquatic sediments. *Applied and Environmental Microbiology,* 31(1), pp. 99-107.

Zeikus, J. G. & Wolfe, R. S., 1973. Fine Structure of Methanobacterium thermoautotrophicum: Effect of Growth Temperature on Morphology and Ultrastructure. *Journal of Bacteriology,* 113(1), pp. 461-467.

Zengler, K. et al., 1999. Methane formation from long-chain alkanes by anaerobic microorganisms. *Nature,* 401(6750), pp. 266-269.

Zhang, T. & Krooss, B. M., 2001. Experimental investigation on the carbon isotope fractionation of methane during gas migration by diffusion through sedimentary rocks at elevated temperature and pressure. *Geochimica et Cosmochimica Acta,* 65(16), pp. 2723-2741.

1. Methane in Pliocene gas accumulations is largely of secondary microbial nature
2. Microbes in the Nile Delta recycle C2+ alkanes arriving from sub-Messinian sources
3. Ethane $\delta^{13}C$ response is buffered unless metabolic rates outpace thermogenic charge
4. Biodegradation pathways are sustained by percolation of C2+ components

Declaration of interests

☒ The authors declare that they have no known competing financial interests or personal relationships that could have appeared to influence the work reported in this paper.

☐The authors declare the following financial interests/personal relationships which may be considered as potential competing interests: